

Review

# Lithium-Ion Capacitors: A Review of Strategies toward Enhancing the Performance of the Activated Carbon Cathode

Obinna Egwu Eleri <sup>1,2</sup>, Fengliu Lou <sup>2,\*</sup> and Zhixin Yu <sup>1,\*</sup> 

<sup>1</sup> Department of Energy and Petroleum Engineering, University of Stavanger, 4036 Stavanger, Norway; obinna@beyondr.no

<sup>2</sup> Beyondr AS, Stokkamyrveien 30, 4313 Sandnes, Norway

\* Correspondence: fengliu@beyondr.no (F.L.); zhixin.yu@uis.no (Z.Y.)

**Abstract:** Lithium-ion capacitors (LiC) are promising hybrid devices bridging the gap between batteries and supercapacitors by offering simultaneous high specific power and specific energy. However, an indispensable critical component in LiC is the capacitive cathode for high power. Activated carbon (AC) is typically the cathode material due to its low cost, abundant raw material for production, sustainability, easily tunable properties, and scalability. However, compared to conventional battery-type cathodes, the low capacity of AC remains a limiting factor for improving the specific energy of LiC to match the battery counterparts. This review discusses recent approaches for achieving high-performance LiC, focusing on the AC cathode. The strategies are discussed with respect to active material property modifications, electrodes, electrolytes, and cell design techniques which have improved the AC's capacity/capacitance, operating potential window, and electrochemical stability. Potential strategies and pathways for improved performance of the AC are pinpointed.

**Keywords:** activated carbon; lithium-ion capacitors; high energy density; high power density and long cycle life



**Citation:** Eleri, O.E.; Lou, F.; Yu, Z. Lithium-Ion Capacitors: A Review of Strategies toward Enhancing the Performance of the Activated Carbon Cathode. *Batteries* **2023**, *9*, 533. <https://doi.org/10.3390/batteries9110533>

Received: 27 September 2023

Revised: 22 October 2023

Accepted: 24 October 2023

Published: 27 October 2023



**Copyright:** © 2023 by the authors. Licensee MDPI, Basel, Switzerland. This article is an open access article distributed under the terms and conditions of the Creative Commons Attribution (CC BY) license (<https://creativecommons.org/licenses/by/4.0/>).

## 1. Introduction

The global transition toward clean and sustainable energy sources has accelerated the electrification of modern-day technologies, particularly in automotive and uninterruptible power supply where fossil fuel energy sources have previously dominated. Energy storage devices, such as lithium-ion batteries (LiB) and supercapacitors (SC), are vital to achieving this rapid transition but are limited by the former's low specific power and the latter's low specific energy [1,2]. However, a breakthrough in 2011 by Amatucci et al. led to the development of a hybrid energy storage device identified as a lithium-ion capacitor (LiC), which combines electrodes from SC and lithium-ion batteries (LiB) as the cathodes and anodes, respectively, while using similar battery-type electrolytes with wide operating potential windows [3]. Therefore, the LiC possessed higher energy density than SC and higher power density than LiB without the self-discharge problems of the former and with a longer cycle life than the latter [3–5].

The demand for lithium has experienced an exponential increase due to the continued electrification of modern society and global population growth. The lithium supply risk has thus necessitated the research and adoption of alternative metals such as sodium, potassium, and aluminum, which can utilize similar mechanisms and reduce the lithium dependence [6,7]. Hence, some of these alternatives will also be discussed in this work, and the strategies outlined can be applied interchangeably.

Conventional SC electrodes incorporated in LiC facilitate high-power densities due to their surface charge storage phenomena [5,8,9]. However, activated carbon (AC) remains the most commercially feasible large-scale alternative compared to other capacitive

cathodes such as graphene, carbon aerogels, carbon nanotubes, and nanofibers due to the complexity associated with incorporating such exquisite cathodes in mass production. On the contrary, AC is favored by the relative ease of fabrication, availability of raw materials, and process scalability. For example, several companies, such as Haycarb, Beyonder, Jacobi, and Norit Carb, have successfully manufactured AC from precursors such as coconut shells, sawdust, and petroleum coke in continuous commercial processes. In addition, other precursors such as algae [10], brewery wastes [11], corncobs [12], tobacco leaves [13], rice husk [14], and lignin [15] have been used to produce high-quality AC in lab-scale research with optimization strategies to synthesize AC from diverse biomass wastes while achieving excellent performance.

AC produced from brewery wastes possessed a surface area of 3600 m<sup>2</sup>/g, pore volumes of 1.8 cm<sup>3</sup>/g, and textural features of visible cavities and open channels inherited from the precursor [11]. The high surface area and accessible pores enabled superior rate performance with minor capacity fade even after a 40-fold increase in the scan rate. The AC produced from the activation of corn cob hydrolysis products is characterized by extensive microporosities with surface areas up to 2300 m<sup>2</sup>/g, pore volumes of 0.93 cm<sup>3</sup>/g, and minimal mesoporosity [12]. Using a two-step activation procedure involving hydrothermal carbonization and subsequent activation, the microstructure of the AC transforms from micrometer-sized spherical particles of varying dimensions to macrometer-sized monolith fragments possessing extensive microporosity. Algae, as a precursor, yields AC with inherent nitrogen doping which can be controlled by optimizing the proteinous nutrients during algae cultivation. However, the porosity of the formed AC is affected by excessive residual metal content which hinders the activation intensity while the inherent nitrogen-doped functionalities are unstable during pyrolysis. Rice husk and tobacco leaves possess inherent silica and atomically dispersed alkali metals, respectively [13,14]. The inherent silica in rice husk enables templated pore creation of beneficial micropores with a narrow pore size distribution while the dispersed alkali metals in tobacco facilitate self-activation by simple carbonization without using externally introduced activation agents. Therefore, the nature of the precursor can significantly influence the properties of the synthesized AC, as will be discussed extensively in Section 2.4.

The renewed focus on sustainable energy storage solutions has spurred interest in carbon-based energy storage devices such as AC/hard carbon (HC) LiC manufactured from sustainable biomass precursors without transition metals. The use of AC as a cathode material is beneficial for achieving sustainable and economical high-powered energy storage devices. For example, wastes and processing by-products such as sawdust and coconut shells, which would have been burnt or deposited in landfills, can be converted into valuable electrode materials for high-power energy storage devices.

When evaluating AC for LiC, the primary parameters considered are its ability to store charge (capacity/capacitance), operating potential range, and electrochemical stability over time. These properties affect the energy, power, and electrochemical stability of the resulting LiC. However, given the non-faradaic surface charge storage phenomena, the AC cathode possesses significantly lower capacity than the faradaic battery-type anode materials incorporated in LiC. Moreover, since the capacity of the LiC is determined by the relation  $1/C_{\text{LiC}} = 1/C_{\text{anode}} + 1/C_{\text{cathode}}$ , increasing the capacity of the AC becomes vital toward increasing the overall capacity of the LiC. The energy density of LiC is also proportional to the capacitance and square of the operating potential window. Wide operating potential windows can facilitate increased energy density but the electrochemical stability of the electrode at the AC surface can limit the performance. Therefore, to improve the performance of LiC, it is necessary to focus on improving the capacity and electrochemical stability of the AC cathode.

Previously, Dubey et al. [16] reviewed various AC synthesis strategies that yielded favorable morphologies for increased power and energy density. Zou et al. [17] reviewed the application of carbon materials in LiCs. However, only a limited section was devoted to the cathode. Han et al. [18] conducted a comprehensive review of material design

strategies and the performance of different cathode and anode material pairs in LiCs. Dos Reis et al. [19] reviewed the application of biomass produced via different synthesis methods in energy storage devices and the effects of their properties on performance. In most of these works, limited attention was devoted to the AC cathode compared to the anode counterparts. Furthermore, in the few reviews highlighting the cathode, the discussion has predominantly been the review of various material synthesis strategies. Here, we discuss strategies regarding the recent progress in material synthesis, electrode, electrolyte, and cell design which have enhanced the performance of the AC cathode incorporated into the LiCs. A schematic of the approach is displayed in Figure 1.

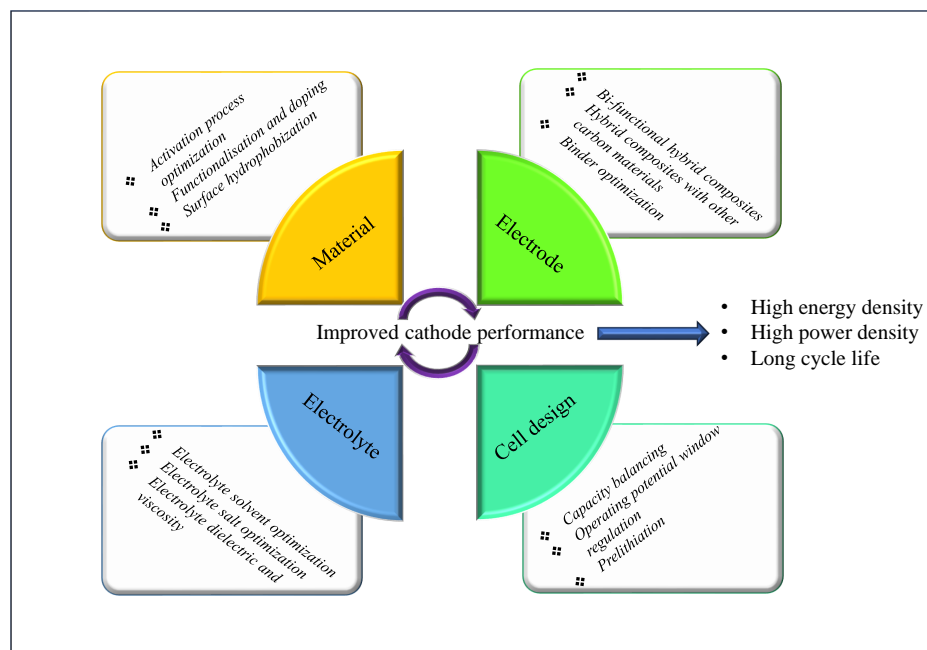


**Figure 1.** Schematic illustrating strategies toward improved performance of the AC cathode.

By not only focusing on the material design, this review provides a broad perspective on enabling the efficient integration of AC in LiC through favorable synergies with other components. The application of these highlighted techniques during the design and fabrication of LiC will facilitate enhanced performance while mitigating potential issues associated with the AC cathode. In the concluding aspect, further areas requiring attention and future research are highlighted.

## 2. Material Optimization

AC is synthesized by subjecting a carbon precursor to a controlled heating procedure in the presence of physical or/and chemical activation agents [20–22]. The nature of the activating agent determines the classification of the activation process, broadly categorized into physical activation, chemical activation, or a combination of the two. Excellent reviews exist on producing AC from various biomass sources using physical or chemical activation processes [23–25]. The activation process aims to produce high surface area materials with tailored pores with dimensions suited to the electrolyte moieties to be adsorbed. Parameters such as the precursor type, activation temperature, activation time, and activating agent concentration are varied during the activation process to optimize the resulting AC's surface area and pore size distribution [13]. The surface area and pore size distribution of the AC correlate with the adsorption capacity for electrolyte moieties given the double layer phenomena, where the obtainable capacitance  $C$  (F) is determined from the equation  $C = \epsilon(A/d)$  [26,27]. The constant  $\epsilon$  represents the product of the electric constant and relative permittivity,  $A$  represents the area of the plates, and  $d$  represents the distance between the plates. Therefore, the amount of charge stored can be converted to capacity

(mAh) by multiplying the capacitance obtained by the potential window. This section will discuss strategies for improving AC's performance enabled by different material optimization techniques.

### 2.1. Activation Process Optimization

AC cathodes, by virtue of the surface charge storage phenomenon, require a high surface area with pores consisting of micropores (<2 nm) for adsorption of electrolyte ions, mesopores (2–50 nm) to facilitate ion diffusion and accessibility to the micropores, and macropores (>50 nm) to serve as electrolyte reservoirs and to enhance ion diffusion to the mesopores and micropores. However, these characteristics necessitated the continuous search for optimum activation procedures initially focused on increasing the surface area and optimizing the pore size distribution. As a result, high specific surface areas of up to  $3000 \text{ m}^2 \text{ g}^{-1}$  were achieved using various chemical activation methods, including KOH activation, combined KOH-KCl activation,  $\text{H}_3\text{PO}_4$  activation, and  $\text{ZnCl}_2$ . Some excellent reviews on the different mechanisms of the activation agents have been published [21–24,28,29]. These high surface area ACs have yielded specific capacitances of up to  $160 \text{ F g}^{-1}$  within the operating potential window of 0–2.7 V in organic electrolytes. However, it was noticed that further increases in surface area do not translate into higher specific capacitance [30]. Furthermore, the extensive activation treatments broaden the pore size distribution, leading to the abundance of ineffective pores that are smaller than the de-solvated electrolyte ion. Moreover, the existing micropores may widen into mesopores due to the intensive gasification of the carbon matrix. The extensive activation also reduces the carbon content in the matrix as numerous mesopores and macropores are created, reducing the density of the AC. This also affects the electrical conductivity due to a large interparticle gap within the carbon structure and a disconnect within the electronic structure. Consequently, low electrode densities often accompany very high specific surface area AC and may result in poor volumetric performance.

Concerning the electrolyte, the high porosity would necessitate increased electrolyte volume in the cells, which may impact the energy density due to the increased weight [4]. Furthermore, the high surface area may also serve as an active site for accelerated electrolyte decomposition, decreasing the cycle life. Khomenko et al. [31] compared the cycle life of two ACs cycled in organic electrolytes. Figure 2a shows the cycling stability tests of two different ACs: Maxsorb and Super 50 with surface areas of  $3487$  and  $1402 \text{ m}^2 \text{ g}^{-1}$  cycled at different upper cut-offs, respectively.

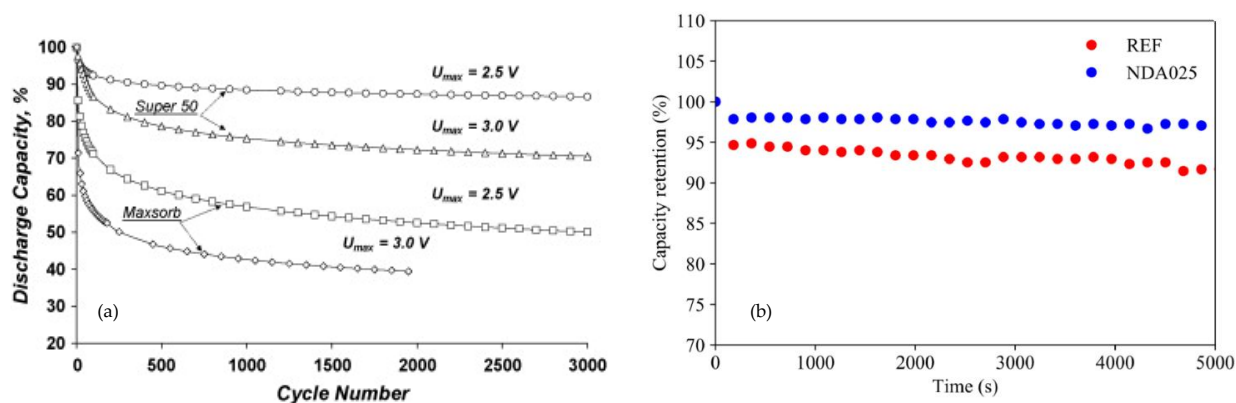


**Figure 2.** (a) Cycle life comparison of Super 50 and Maxsorb using 1 M  $\text{Et}_4\text{NBF}_4$  in acetonitrile. The cells are cycled with different cut-off voltages ( $U_{max}$ ) at a current density of  $650 \text{ mA g}^{-1}$ . Reprinted from [31], copyright (2008), with permission from Elsevier. (b) Cycle life comparison of AC produced by a modified activation method (NDA025) and the reference sample (REF) using 1 M  $\text{TEABF}_4$  in PC. Retrieved from [32], copyright (2020), with permission from Elsevier.

The results in Figure 2a revealed that the AC with the highest surface area had the highest capacity fade. Although a high surface area is required for adsorption, carefully controlled activation procedures are necessary to modulate the surface area and create pores with diameters similar to the electrolyte ions. An AC with pores of similar diameters to the electrolyte ions was reported to have increased capacitance [33]. The discovery that ions could access pores smaller than the solvated ion size further underscores the need for the activation of process optimization [34]. Likewise, controlled mesoporosity formation and tailored microporosity could facilitate increased volumetric performance through enhanced electrode densities.

Several activation techniques have recently yielded ACs with superior gravimetric and volumetric electrochemical performance beyond the typical physical or chemical activation procedure with steam or singular chemical agents. Eleri et al. [32] used a non-destructive activation method to synthesize high-performance AC from sawdust with reduced defects, high surface area, increased microporosity, and high electrode density with optimized mesoporosity. The non-destructive activation (NDA) method incorporated an Al additive in KOH chemical activation acting as an oxygen scavenger to reduce the oxides' extensive gasification of the carbon matrix. The modified activation procedure ensured that exfoliation due to potassium intercalation into the carbon matrix was the dominant mechanism, creating more micropores and reducing gasification-induced mesoporosity. The NDA carbon also exhibited superior performance in the cycling stability test than the reference sample as shown in Figure 2b. The improved performance can be attributed to reduced defective sites on the NDA carbon which are active sites upon which electrolyte degradation is accelerated compared to the reference sample. Zheng et al. [35] incorporated a surfactant-modified KOH activation process in synthesizing in situ nitrogen-doped activated porous carbons with a controlled pore size, which could function as dual anode and cathode materials in a 4.5 V LiC. The porous carbon was obtained from the carbonization of polypyrrole (PPy) prepared with the surfactant cetyltrimethylammonium bromide (CTAB) and subsequent KOH activation of the carbonized material. The surfactant-modified KOH activation process influenced the pore size distribution of the carbon by creating mesopores in the spaces occupied by the decomposed surfactant and controlling the porosity formation. Specific capacities reaching 80 mAh g<sup>-1</sup> at 0.1 A g<sup>-1</sup> in the potential window 2–4.5 V were achieved using this material in the half-cell configuration with 1M LiPF<sub>6</sub> EC:DEC (1:1) vol% electrolyte. On the contrary, the AC synthesized without the surfactant possessed a higher surface area (2528.0 m<sup>2</sup> g<sup>-1</sup> compared to 1894.9 m<sup>2</sup> g<sup>-1</sup>) but poor electrochemical performance due to hindered ion diffusion, nonuniform pore size distribution, and ineffective micropores. Again, this further amplifies the need for optimized pore size distributions in contrast with solely achieving high surface area through extensive activation.

AC is structurally classified as an amorphous disordered material that relies on ion adsorption/desorption as the charge storage mechanism. However, it has been demonstrated that introducing some degree of ordered structures through partial graphitization while maintaining sufficient porosity can also increase the capacity of the AC by enabling intercalation within the ordered structure. Sun et al. [36] synthesized an ordered–disordered hybrid AC cathode as opposed to the typical disordered AC. The ordered–disordered hybrid AC was produced by simultaneous nitrogen doping, in situ graphitization, and subsequent activation of a Ni and Zn citrate composite prepared using a one-step solvothermal route. A schematic of the activation procedure is shown in Figure 3a.

The graphitization degree was controlled by modifying the ratio of the incorporated Zn and Ni elements. The latter two were subsequently removed by acid leaching after the activation process. High-resolution transition electron microscopy (HR-TEM) images of the produced AC showing the ordered structure surrounded by an amorphous phase are presented in Figure 3b–d. The ordered–disordered AC enabled dual charge storage mechanisms through anion intercalation and the typical adsorption and desorption, realizing a specific capacity of 130 mAh g<sup>-1</sup> in the potential window 2–4.6 V. The assembled LiC had an energy density of 23.5 Wh kg<sup>-1</sup> at a power density of 40.6 W kg<sup>-1</sup>. Moreover, the

presence of the ordered structure also decreased the self-discharge while the porous and amorphous nature alleviated the volume swelling commonly encountered in ordered carbon. Cho et al. [37] also developed similar ordered–disordered carbon, named as partially graphitic carbon, which combined shallow intercalation and double-layer adsorption as the charge storage mechanism.

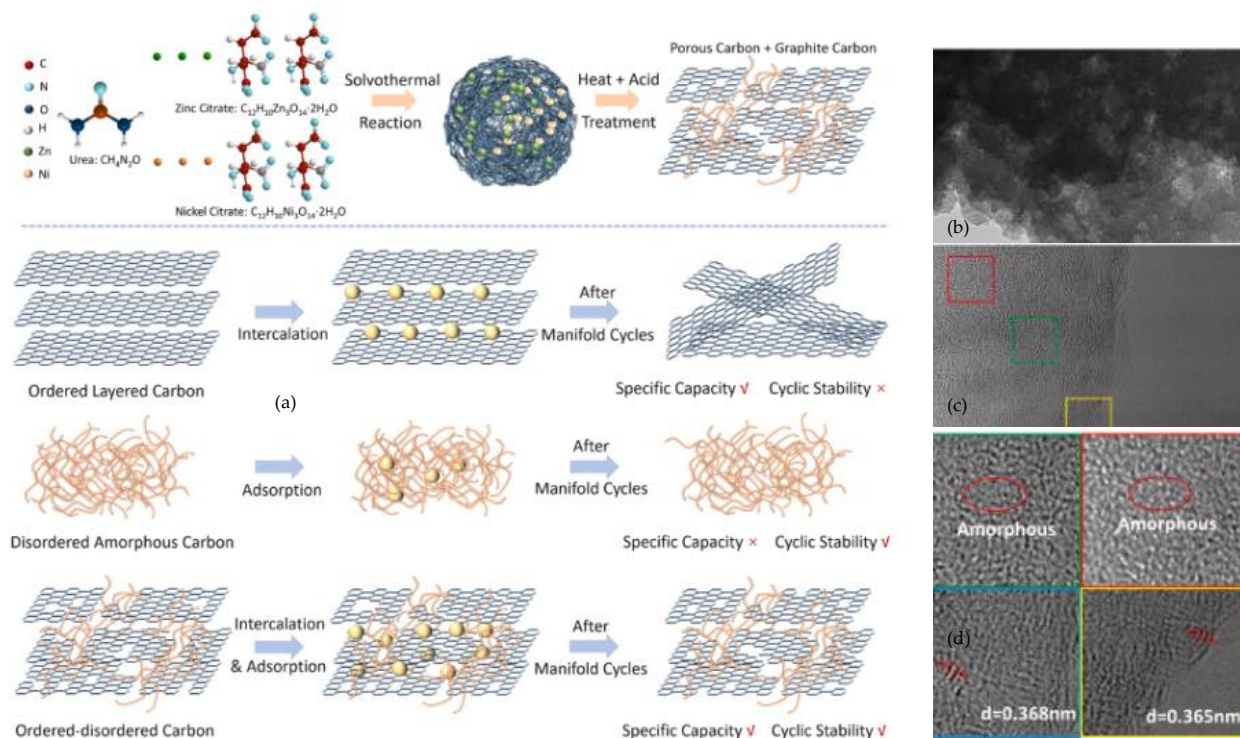


**Figure 3.** (a) Schematic of the preparation procedure. (b–d) High-resolution transition electron microscopy (HR-TEM) images of the prepared ordered–disordered carbon. Reprinted from [36], copyright (2022) with permission from Elsevier.

In a notable work, Jain et al. [38] reported on the synthesis of a high specific surface area and mesoporosity-rich AC that achieved a specific capacity of  $70 \text{ mAh g}^{-1}$  in the potential window of 2.0–4.0 V using the electrolyte 1M LiPF<sub>6</sub> in EC:DMC (1:1). The AC was produced using a modified ZnCl<sub>2</sub> activation method. The precursor material was pre-treated with H<sub>2</sub>O<sub>2</sub> and then hydrothermally carbonized in an autoclave. The carbonized material was impregnated with ZnCl<sub>2</sub> and a processing agent benzene tetracarboxylic acid (BTA) before drying and subsequent activation. The pre-treatment step with H<sub>2</sub>O<sub>2</sub> enhanced the mesoporosity and the oxygenated surface functionalities onto the carbonized material while the processing agent BTA enabled increased mesopore surface area during activation. Furthermore, the introduced surface functionalities improved the efficacy of the ZnCl<sub>2</sub> activation agent by promoting nucleophilic attraction of the Zn<sup>2+</sup> to the free electron pairs of the oxygen atoms, thereby ensuring greater access to the precursor surface and facilitating dehydration of the biomass material in the activation step.

## 2.2. Functionalization and Doping

The nature of chemical functionalities at the surface and doped elements within the carbon matrix can influence the electrochemical performance of AC. Surface functionalities could be inherited from the precursor material or deliberately introduced during the activation or post-treatment activation procedures. As a result, benefits such as enhanced conductivity, improved wettability, and increased active sites for pseudocapacitive Li<sup>+</sup> storage can be obtained [39]. This section discusses the effect of heteroatoms such as N, B, O, F, S, and P on the AC's performance in nonaqueous electrolytes.

### 2.2.1. Nitrogen

Nitrogen functionalization has been particularly popular due to improved charge carrier transport caused by increased contributions of p- electrons to the  $\Pi$  system following the positive synergy between the N atom and carbon lattice [39–41]. This therefore enables an increased sorption capacity toward the anion when combined with appropriate pore size distributions [42,43]. The electron-donating abilities induced by nitrogen functionalization create additional electroactive sites, thereby improving the AC's electrochemical reactivity, surface polarity, electrical conductivity, and wettability [44]. Li et al. [45] synthesized nitrogen-doped AC from corn cobs with a very high surface area of up to  $2900 \text{ m}^2 \text{ g}^{-1}$ . The nitrogen-doped AC exhibited an initial specific capacity of  $129 \text{ mAh g}^{-1}$  at  $0.4 \text{ A g}^{-1}$  in the half-cell configuration using an organic electrolyte and operating potential window of 2–4.5 V. Yang et al. [46] synthesized nitrogen-doped porous carbons using urea as nitrogen dopant and glucose as a precursor. The nitrogen-doped porous carbon realized a specific capacity of  $62 \text{ mAh g}^{-1}$  in the potential window 3–4.6 V compared to  $38 \text{ mAh g}^{-1}$  obtained from a commercial AC at similar conditions. Furthermore, specific energies of  $83.25 \text{ W h kg}^{-1}$  at a  $25 \text{ kW kg}^{-1}$  power density were achieved using the nitrogen-doped porous carbon as the cathode and MnO-graphene composite as the anode. The impressive performance was attributed to the well-developed interconnected pore structure and active N-sites in the AC that facilitated capacitive and redox reactions during charge storage. Lota et al. [43] investigated the influence of nitrogen content in AC samples on the performance of capacitor systems using aqueous and organic electrolytes. A clear correlation between increased capacities and nitrogen content was obtained in aqueous media. However, in the organic media, increased nitrogen content resulted in a capacitance increase only when matched with appropriate pore size distribution.

### 2.2.2. Boron

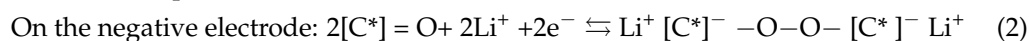
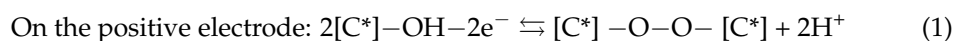
Boron functionalization is another method of increasing the electrochemical reactivity of the AC by modifying the carbon electronic structure. Functionalization with boron increases the density of charge carriers in the carbon matrix after the substitution and improves the electronic conductivity due to the p-type characteristics [47]. Since boron atoms possess one electron deficient in the valence layer and are less electronegative than carbon, the presence of boron (an electron acceptor) in the carbon matrix induces a shift in the fermi level to the conducting band, thereby modifying the carbon electronic structure and improving properties related to the electrochemical efficiency and chemical reactivity [48–50]. Furthermore, the crystallinity of the carbon structure is improved and the oxidation rate of the matrix is lower due to the decreased electroactive sites for oxygen chemisorption [49–52]. Boron functionalization and the consequent formation of borates on the carbon structure also reportedly induce pseudocapacitive charge storage on the carbon surface [51] together with the improved electrical conductivity of the electrode that enhances the high-rate performance.

Jiang et al. [53] reported the effect of dual doping of boron and nitrogen on the performance of LiC in organic electrolytes. Doping with boron enabled a widened operating potential window of up to 4.8 V and improved electrode conductivities and electrochemical performance. Furthermore, the presence of boron atoms on the cathode promoted the adsorption of  $\text{PF}_6$  anions, as revealed by DFT calculations of the adsorption energy. The boron-doped cathode possessed lower adsorption energy compared to the undoped alternative. Therefore, the electropositive boron atoms created a net positive charge on the electrode and, in that way, reinforced the ability of the electrode to lose electrons while facilitating the intense attraction of the  $\text{PF}_6$  anion. Consequentially, incorporating the boron-doped cathode in the LiC architecture delivered a specific energy of  $200 \text{ Wh kg}^{-1}$  at  $239.9 \text{ W kg}^{-1}$  with a capacity retention of 80% after 7000 cycles. Zhu et al. [54] obtained a high capacity of  $190.2 \text{ mAh g}^{-1}$  after dual boron–nitrogen doping of a zinc ion capacitor cathode. The dual doping strategy increased anion adsorption and chemical interactions with  $\text{Zn}^{2+}$  at the electrode/electrolyte interface.

### 2.2.3. Oxygen

Surface oxygen functionalities present a dilemma for AC regarding irreversible or reversible redox reactions with the nonaqueous electrolytes commonly used in LiC. Liu et al. [55] reported that oxygen functionalization facilitated improved capacitance in AC electrodes used in LiC. Commercial ACs were functionalized by ammonium persulfate and sulfuric acid treatment. The functionalized AC displayed superior capacities of  $78 \text{ mAh g}^{-1}$  when tested in half cells with a lithium counter electrode and an organic electrolyte of 1 M LiTFMS/diglyme. The authors proposed that the improved performance was caused by reversible pseudocapacitive reactions between  $\text{Li}^+$  ions and C=O functional groups introduced after the functionalization treatment. However, the functionalized AC displayed lower capacity retention during continuous cycling than the pristine AC. This behavior was further attributed to detrimental irreversible redox processes which may have contributed to lower cyclic stability. Moreover, these redox processes were assumed to be finite and occurred during a transition period in the first few cycles, beyond which stable cycling was attained. A related study by Li et al. [56] also using ammonium persulfate and sulfuric acid functionalization of a commercial AC, revealed that oxygen functionalities improved the performance in the aqueous 6 M KOH electrolyte but not the organic electrolyte 1M  $\text{Et}_4\text{NBF}_4/\text{PC}$ , as shown in Figure 4a. Therefore, the beneficial effect of oxygen functionalities concerning nonaqueous electrolytes may be restricted to AC electrodes cycled in electrolytes with  $\text{Li}^+$  ions as the adsorbed/desorbed species during charge storage. This was further demonstrated by Zhang et al. [57] who used the electrolyte 1 M  $\text{LiPF}_6$  in EC:EMC (3:7). The effect of surface oxygen functionalities of the AC was investigated in lithium half cells and symmetric AC/AC cells. It was interesting to observe the positive pseudocapacitive impact of oxygen functionalities arising from faradaic reactions with  $\text{Li}^+$  ions. The charge and discharge potential profile of the AC electrode with 4.26 wt.% oxygen was examined in the three-electrode configuration. Figure 4b,c shows the potential profiles in the first cycle sweep obtained from different electrolytes. Three regions are identified which correspond to incremental capacity by adsorption/desorption in I, combined adsorption/desorption and pseudocapacitance in II, and irreversible oxidation/reduction in the electrolyte solvent in III.

The Initial reactions between the surface oxygen functionalities and electrolyte moieties affect the initial coulombic efficiency, capacitance retention, potential profile, and subsequent formation of soluble redox products such as organic and hydrogen peroxides. These redox products can shuttle between the positive and negative electrodes due to their strong coordinating ability to  $\text{Li}^+$ . Furthermore, changes in the electrolyte solubility arising from the continued accumulation of such redox products may cause the precipitation of insoluble deposits (lithium salts) at the AC surface, thereby blocking the pores and accessible surface area and reducing the capacity of the AC. The irreversible reactions can be identified by the deviation of the charge and discharge profile from the expected linear lines due to the reversible double-layer adsorption and desorption of electrolyte ions. Nevertheless, the potential profile of the AC gradually reverts to a linear shape upon continued cycling due to the depletion of the irreversible surface oxygen functionalities and the formation of a protective solid electrolyte interface layer. Pseudocapacitive reactions with surface oxygen functionalities of the AC are proposed to occur via the following reactions (1)–(4) [57]:



where  $[\text{C}^*]$  represents the  $\text{sp}^2$  carbon situated at the edges of the graphene moieties capable of delocalizing the charge. Equations (1) and (2) are reversible processes responsible for the pseudocapacitance through reactions of the surface oxygen bonded to the graphene moieties capable of delocalizing charge. However, Equation (3) expresses the irreversible

formation of an insoluble lithium salt which is terminated by the reaction described in Equation (4). The expression  $R_1-O-O-R_2$  represents probable soluble redox species such as organic peroxides and hydrogen peroxide, where  $R_1$  and  $R_2$  are organic functional groups inherent to the AC's surface chemistry. Therefore, Equations (3) and (4) postulate the irreversible reactions responsible for the low initial coulombic efficiency in the first and subsequent cycles prior to depletion of the surface functionalities.

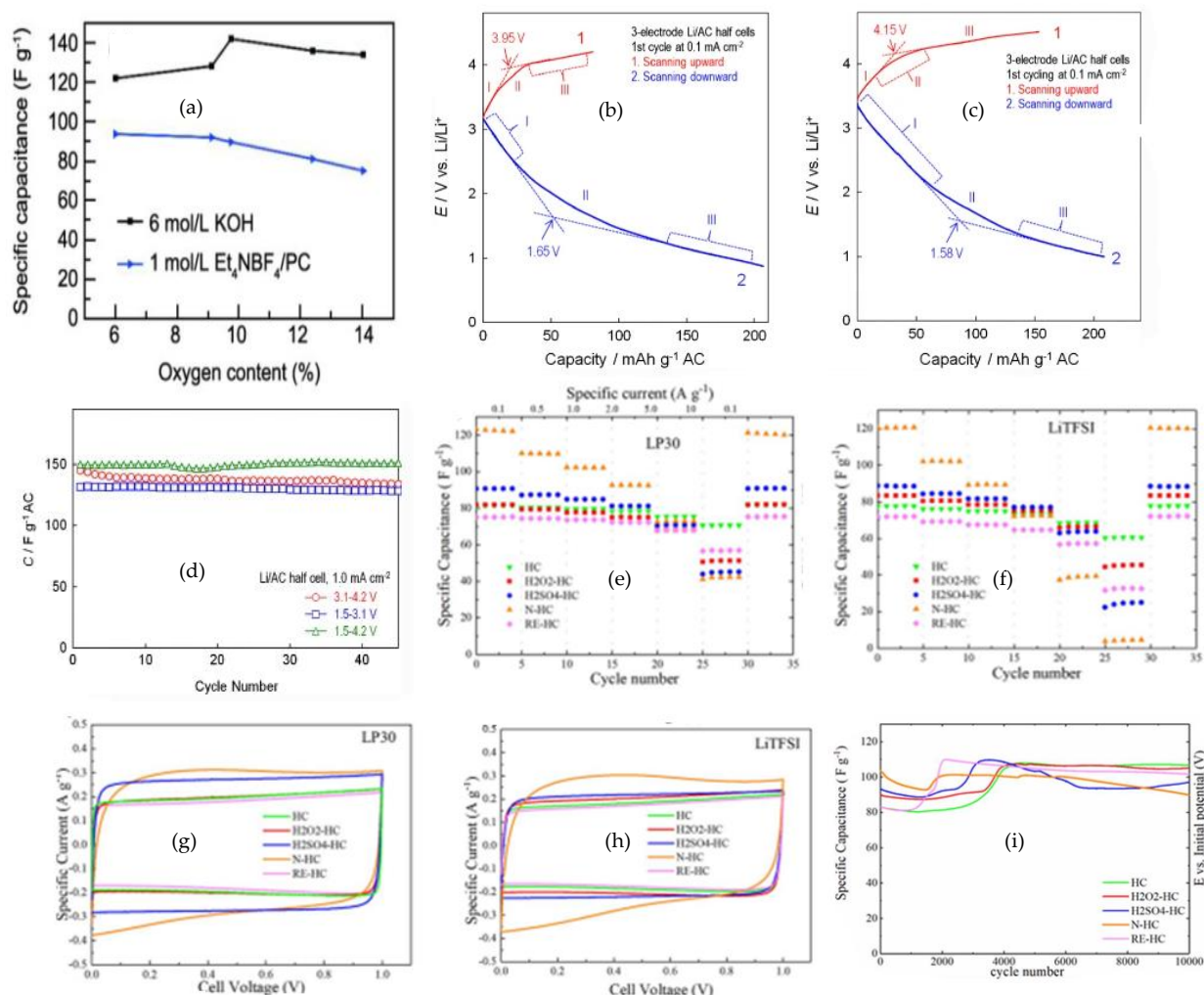


**Figure 4.** (a) Effect of oxygen content on cycle life in organic and aqueous electrolytes, reprinted from [56], copyright (2020), with permission from Elsevier. First cycle charge and discharge profile of fresh AC electrodes using three-electrode cell configuration with a lithium reference electrode in (b) 1M  $\text{LiPF}_6$  in EC/DMC (3:7) electrolyte and (c) 1M  $\text{TBABF}_4$  in EC/DMC (3:7) electrolyte. (d) Comparison of cycle life at different potential windows, reprinted from [57], copyright (2017), with permission from Springer. Effect of various surface functionalities on the performance of the AC in (e) LP30 and (f) LiTFSI electrolytes. Cyclic voltammety obtained using (g) LP30 and (h) LiTFSI electrolyte. (i) Effect of surface functionalities on the cycle life, reprinted from [58] (CC-BY).

To confirm the existence of the reversible pseudocapacitive phenomena, three potential windows were examined that encompassed  $\text{PF}_6$  adsorption and desorption (3.1–4.2 V) above the open circuit potential (OCP), Li adsorption and desorption below the OCP (1.5–3.1 V), and combined  $\text{PF}_6$  and lithium adsorption/desorption (1.5–4.2 V), as presented in Figure 4d. From Figure 4d, expectedly, the widest potential window (1.5–4.2 V) exhibited the largest capacitance of  $150 \text{ F g}^{-1}$ . On the other hand, the potential window (3.1–4.2 V) had a slightly increased initial capacitance than 1.5–3.1 V but later stabilized to similar values. Since the AC specific capacitance by double layer adsorption and desorption

is independent of the potential window, the increased capacitance using 1.5–4.2 V can undoubtedly be attributed to reversible pseudocapacitance through equations 1 and 2. Therefore, oxygen functionalities have been demonstrated to be beneficial by facilitating capacitance increase through pseudocapacitance [57].

Ding et al. [58] further validated the existence of pseudocapacitive reactions with oxygen functionalities that could influence the capacitance of AC cycled in nonaqueous electrolytes of lithium salts. In this work, a commercial AC was functionalized by deliberate treatment with nitric acid, sulfuric acid, hydrogen peroxide, and di-functionalized via heat treatment under hydrogen/argon gas. Figure 4e,f shows the results from the electrochemical testing of these samples in 1M LiPF<sub>6</sub> in EC:DMC(1:1) (LP30) and 1M LiTFSI in EC:DMC(1:1) (LiTFSI) electrolytes. The beneficial effects of surface oxygen functionalities were again demonstrated by an increase in the AC-specific capacitance through pseudocapacitance. All the functionalized AC had a lower surface area than the di-functionalized AC due to the oxidation treatment. However, despite the higher surface area of the di-functionalized AC, the functionalized AC had much higher specific capacitance even with the lower surface area. Furthermore, the nitric acid-treated AC had the highest capacitance and C=O groups among the functionalized samples. The effect of surface functionalities was also noted in the investigated electrolyte stability windows, as shown in Figure 4g,h. The di-functionalized AC had the narrowest electrolyte stability window due to the higher number of reactive sites caused by the hydrogen reduction treatment. Among the functionalized samples, the nitric acid-treated AC had the narrowest electrolyte stability window, which can be related to the C=O groups at the surface. Therefore, functionalization can increase the specific capacitance through reversible pseudocapacitance but may also impact the electrolyte stability window. Meanwhile, the absence of stabilized functional groups at the surface following reductive treatment would create highly reactive sites that can accelerate electrolyte decomposition and reduce the electrolyte stability window. This work further confirmed that the pseudocapacitive behavior was related to Li<sup>+</sup> ions and that the respective anions do not partake in the pseudocapacitive reactions [58]. Additionally, intermediate surface oxidation with the optimum oxygen functionalities can ensure increased capacitance through pseudocapacitance without negatively impacting the cycle life. Nevertheless, the specific content or nature of oxygenated surface functionalities that can facilitate pseudocapacitance without affecting long-term cyclability through irreversible faradaic reactions remains a question to be answered. The results from the cycling stability test conducted on these samples are presented in Figure 4i. During the cycling stability tests, the H<sub>2</sub>O<sub>2</sub>-treated AC had the highest capacitance retention rate which was superior to the pristine AC or difunctionalized AC. Meanwhile, the nitric acid-treated AC with more C=O functionalities had the lowest capacity retention rate during the long-term cycling.

#### 2.2.4. Fluorine

Fluorine functionalization has been reported to facilitate improved affinity for organic electrolyte ions on the AC surface [59]. Doping with fluorine amplifies the electroactive sites and impacts some electronegativity onto the carbon surface. Zhou et al. [59] synthesized fluorine-doped AC that achieved a high specific capacitance of 168 F g<sup>-1</sup> using an organic electrolyte 1M tetraethylammonium tetrafluoroborate in propylene carbonate (1M TEA BF<sub>4</sub> in PC) and symmetric cell configuration. The improved performance with high fluorine content was caused by the synergy between increased surface area and favorable surface chemistry. DFT calculations showed that the affinity for the TEA<sup>+</sup> ions was increased with fluorine doping compared to the pristine material. However, the existence of pseudocapacitive contributions of fluorine is yet to be confirmed.

#### 2.2.5. Phosphorous

The electron-donating ability and large covalent radius of phosphorous make it an attractive heteroatom for doping carbon matrices. Phosphorous doping was reported to facilitate improved performance through enhanced pseudocapacitive reactions and improved

electronic conductivity caused by the electron-donating ability of phosphorous [60,61]. In addition, the much larger covalent radius of phosphorus ( $107 \pm 3$  pm) compared to carbon ( $73 \pm 1$  pm) creates defects on the carbon surface after doping [62]. These defects may serve as active sites where charges are concentrated, facilitating charge transfer reactions [61]. Furthermore, phosphorous doping expands the interlayer spacing of the carbon lattice due to the larger atomic radius than the carbon matrix, thereby favoring more adsorption of sodium or lithium ions [63,64]. Gao et al. [60] synthesized AC from starch, using phytic acid as an activation agent and phosphorous dopant. The AC displayed a high specific capacity of  $81.7 \text{ mAh g}^{-1}$  at  $0.05 \text{ A g}^{-1}$  and good rate capability in the potential window 2–4 V in Li half cells using 1M  $\text{LiPF}_6$  in EC:DMC:EMC (1:1:1) electrolyte. The high capacity achieved was attributed to the combined effect of pseudocapacitance and electrochemical double-layer capacitance from the synergy between the appropriate pore size distribution and high phosphorous content.

#### 2.2.6. Sulfur

Sulfur functionalization on the AC surface induces electron delocalization of carbon backbones, thereby creating more electroactive sites that increase wettability and improve conductivity. The electron delocalization occurs due to the overlap between an electron pair on the p-orbital in sulfur and the  $\Pi$  orbital of the  $sp^2$  hybridized sites in the AC. Sulfur-containing materials, like thioglycolic acid and thiourea, can be used as dopants to impact sulfur functionalities in carbon matrixes. Thangavel et al. [65] obtained a specific capacitance of  $252 \text{ F g}^{-1}$  at  $0.5 \text{ A g}^{-1}$  in a sodium ion capacitor after nitrogen and sulfur codoping of the cathode with thiourea. The improved performance was attributed to the enhanced synergetic effect of the dual heteroatom elements. The sulfur heteroatoms enhanced the space utilization and promoted the electrosorption of the electrolyte ions while nitrogen enabled increased electron transport and rapid ion transport kinetics inside the pores [65–67].

Different heteroatoms have been reviewed in the previous section, highlighting the improved AC performance through enhanced space utilization, decreased adsorption potentials, or pseudocapacitance during charge storage. Heteroatoms such as oxygen, phosphorus, nitrogen, and boron have reportedly exhibited increased capacitance through pseudocapacitance, although to varying degrees. Moreover, the positive pseudocapacitive effect is mainly observed while using aqueous electrolytes. However, pseudocapacitance has also been reported in organic electrolytes, particularly when matched with appropriate pore size dimensions. A capacitance increase is often accompanied by decreased cycling stability for heteroatoms like oxygen. On the contrary, nitrogen, boron, and phosphorus exhibit pseudocapacitance without the accompanying loss in cycling stability. The pseudocapacitive effects of fluorine and sulfur remain unconfirmed, but they are beneficial for enhancing space utilization, improving surface chemistry, and promoting the electrosorption of electrolyte ions.

In summary, heteroatom doping in the carbon matrix can improve the performance of the AC through various means. However, further studies are needed to compare the efficacy of heteroatom doping in organic electrolyte systems, in particular, using Li-ion or other alkali metal ion salt that can exhibit peculiar pseudocapacitive behaviors with surface functionalities.

#### 2.3. Surface Hydrophobization

The interactions between the electrolyte solvent and active material surface can influence the performance of the electrochemical energy storage devices. The wettability can affect the surface area utilization and accessibility to the pores. Poor wettability can result in high internal resistance and lower capacitance despite the capacitive material possessing sufficient surface area and pores [68–71]. Hence, increasing the wettability is an efficient technique to improve the performance of the AC. Wei et al. [71] demonstrated a unique approach to increasing the wettability of active materials in organic electrolytes

through surface modification with a surfactant (sodium oleate). The surfactant enabled the attachment of non-polar organic functional groups to the AC surface, thereby increasing the surface hydrophobicity and affinity to the organic solvent. The modified material consequentially displayed improved capacitance, reduced internal resistance, and higher energy and powder densities than the unmodified material. Similarly, improved performance through surface modifications using Vinyltrimethoxysilane surfactant has also been reported [70,72]. Surface modifiers containing the silane functional group with only a methyl and alkoxy group bonded to the silicon atom can effectively facilitate increased hydrophobicity at the surface. Nevertheless, the surface modification process can reduce the AC's surface area and limit accessibility to the pores if the grafted surface modifiers possess too large a molecular size.

#### 2.4. Precursor Optimization

Precursor materials can affect the final properties of the produced AC. Parameters such as the carbon content, organic and inorganic matter content, heteroatoms, precursor carbon structure, and the interactions between the precursor carbon matrix and activation agent would determine the qualities of the synthesized activated carbon [22]. AC produced from naturally occurring precursors, such as biomass materials, often retain the inherent structure of the original biomass material. The activation process typically occurs via crosslinking, dehydration, exfoliation, or gasification of the precursor matrix depending on the type of activation agent [73]. These processes are broadly summarized by the reduction in the oxygen content of the precursor through the removal of volatiles and moisture as well as some of the precursor's carbon content as the pores are being created. The precursor's carbon, oxygen, and volatile matter content can therefore affect the efficacy of the activation process [22]. The activation agent is often more attracted to the oxygen radicals of the precursor, thereby increasing the activation intensity and reducing the activation duration needed for achieving particular burn-off rates. Precursor materials with high volatile content, such as biomass-based materials, often possess higher surface areas than synthetic materials (e.g., organic polymers) [22,74]. Although the removal of volatiles during the carbonization/pyrolysis process is strongly related to the activation temperature, the macrostructure and nature of crosslinks between the precursor crystallites can affect the diffusion of the activation agent, which in turn dictates the porosity formation [75]. Precursors containing crystallite structures with several aromatic layers are reportedly more difficult to activate due to stronger covalent bonds among the carbon atoms in the layers [76]. In contrast, precursors containing carbon atoms with unsaturated bonds (mainly at the edge) are considerably more reactive and easily activated [76].

Comparing biomass-based precursors and others such as petroleum coke, residues, and synthetic organic polymers, the former possesses relatively higher ash content and inorganic impurities from fertilizers and nutrients absorbed from the soil. The latter is somewhat purer with low inorganic contents and often results in AC with higher yields due to the increased carbon content. However, high ash content and mineral impurities are detrimental to the performance of the AC. Their presence in the AC can lead to high self-discharge and poor electrochemical cycling stability, attributed to parasitic reactions between the metals and electrolytes [77]. Moreover, the high ash content in the precursor can reduce the effect of the activation agent, thereby hindering pore formation and necessitating high concentrations of the activation agent to achieve the desired activation degree [78].

The precursor can also influence the surface chemical functionalities and heteroatoms present in the AC. Several biomass precursors possess heteroatoms, such as nitrogen, sulfur, and the typical carbon, hydrogen, and oxygen, as elemental constituents. Li et al. [79] synthesized high-performance N-doped AC (8 wt.% N) with a hierarchical porous structure from eggshells (possessing 12–15 wt.% N) by simple carbonization without any doping agent. Naturally N-doped AC has also been synthesized from silk fibroins [80,81], fish scales [82], and prawn shells [83]. Biomass protein precursors, such as broad beans and

chicken bones, contain sulfur and can produce sulfur-doped AC [66,84]. Fruit seeds and pulps are excellent natural phosphorous dopants [85].

Some precursor materials can also undergo self-activation without the need for activation agents. The absence of activation agents can enable controlled porosity generation in the AC with well-distributed pores. Klezyk et al. [13] synthesized AC from tobacco leaves and stem wastes without any activation agent. The synthesized AC had a narrow pore size distribution and excellent electrochemical performance in both aqueous and organic electrolytes. The success of the self-activation could be linked to the presence of well-distributed alkalis in the precursor on the atomic scale. Moreover, the evolved gases during the carbonization treatment can simultaneously participate in the activation process during the carbonization step. Therefore, self-activating precursors present a facile approach toward achieving narrow pore distribution due to the atomically dispersed nature of the alkali metals and the absence of external activation agents that may contribute to uncontrollable gasification rates. Similar self-activating abilities have been demonstrated by seaweed and proposed to occur in biomass precursors that contain naturally embedded elements such as Na, K, Ca, and Mg [86]. Synthetic materials such as polyvinylidene chloride have also demonstrated excellent self-activating properties, achieving high-performance AC without an additional activation step [87].

Atomically dispersed elements in precursors have also aided the activation process by serving as templates during porosity formation. Xue et al. [14] reported that the templating behavior exhibited by silica present in rice husk precursors during the synthesis of AC. The silica nanoparticles were selectively leached using NaOH and KOH treatment before activation. A detailed study was conducted on the effectiveness of silica embedded in the rice husk and on the surface. Nanoparticle silica embedded in the rice husk was revealed to favor porosity formation through a templating and synergetic effect with alkali activators that ensured more active sites during activation. In contrast, the silica present at the surface reduced the efficiency of the activation agent and the produced AC had decreased porosity and a decreased templating effect. Niu et al. [88] reported the self-activating effect of hydroxyapatite found in animal bones which enabled the synthesis of high-performance cathodes ( $109 \text{ mAh g}^{-1}$  at  $0.1 \text{ A g}^{-1}$  in the potential window 2.0–4.5 V) after a simple pyrolysis step.

In summary, the precursor's nature can affect AC's quality. Other notable works synthesizing high-quality AC from different precursors are summarized in the following. Quian et al. [89] synthesized high-performance AC from petroleum asphalt using potassium bicarbonate as an activation agent. The AC had a specific capacity of  $92 \text{ mAh g}^{-1}$  at  $0.1 \text{ A g}^{-1}$  in the operating potential window 2.0–4.5 V using the electrolyte 1 M  $\text{LiPF}_6$  in EC:DMC:EMC(1:1:1) vol%. Yang et al. [90] synthesized AC from corn cobs using sulfuric acid as an activation agent. The obtained AC possessed a specific capacitance of  $251 \text{ F g}^{-1}$  at  $0.3 \text{ A g}^{-1}$  in the operating potential window 2.0–4.5 V while using the electrolyte 1 M  $\text{LiPF}_6$  in EC:DMC(1:1). Sennu et al. [91] synthesized AC from *Prosopis juliflora* using the typical KOH activation at  $900 \text{ }^\circ\text{C}$ . The produced AC had in situ heteroatoms from the precursor (N, S, and Ca) which enabled a specific capacity of  $98 \text{ mAh g}^{-1}$  at  $0.1 \text{ A g}^{-1}$  in the operating potential window 2.0–4.0 V.

### 3. Electrode Optimization

After synthesizing the active material, the electrode is the next critical step influencing performance. During electrode fabrication, the AC powder is mixed with selected binders, ensuring good adhesion between the particles and the current collector. Moreover, the electrode can be fabricated with a dissolving solvent to aid the dispersion of the particles, binder, and additive composites which are often introduced to optimize the performance. This section discusses the influence of parameters such as binders and hybrid composites consisting of carbon materials or high-capacity bi-functional cathodes on the performance of the AC.

### 3.1. Bi-Functional Hybrid Composites

Despite the advances in the activation process discussed previously, the capacity of AC remains limited compared to intercalation-type battery cathodes like lithium iron phosphate (LFP) ( $160 \text{ mAh g}^{-1}$ ). Recently, researchers have implemented composite mixtures of AC with conventional battery-type materials as bi-functional hybrid cathodes to increase the capacity and energy density of the LiC cathode. Benefits such as increased cathode composite conductivity, improved rate performance, enhanced power, and energy density were obtained when these hybrid composite electrodes were integrated into the LiC architecture. Chen et al. [92] used a hybrid cathode mixture consisting of AC and  $\text{LiNi}_{0.6}\text{Co}_{0.2}\text{Mn}_{0.2}\text{O}_2$  (NCM) and HC as the anode to achieve simultaneous higher power and energy density than the conventional NCM/HC battery at high C-rates. The improved energy and power density of the hybrid cathode were ascribed to the properties of the AC, such as mesoporosity, surface area, and enhanced electrode conductivity. The mesopores served as electrolyte reservoirs facilitating fast lithium diffusion while the high surface area contributed to the increased capacity through double-layer charging. However, optimizing the AC content in the electrode was essential to achieving such improved capacity. Shellikeri et al. [93] investigated the performance of an AC/LFP (80/20) wt.% bi-functional cathode paired with a pre-lithiated HC anode in the fabrication of LiC. SEM images obtained from the hybrid cathode are presented in Figure 5a. The AC occupied the spaces between the LFP particles which promoted faster kinetics during charge and discharge at high c-rates. Three-electrode cell measurements probed the individual capacity profiles of the electrodes, as presented in Figure 5b. The cathode exhibited a dual charge storage mechanism, with the capacity contribution in zone a (2.2–3.45 V) and c (3.45–3.8 V) due to the AC while zone c with the plateau at 3.45 V is from the LFP. Cycling stability tests conducted on the hybrid cathode are presented in Figure 5c.

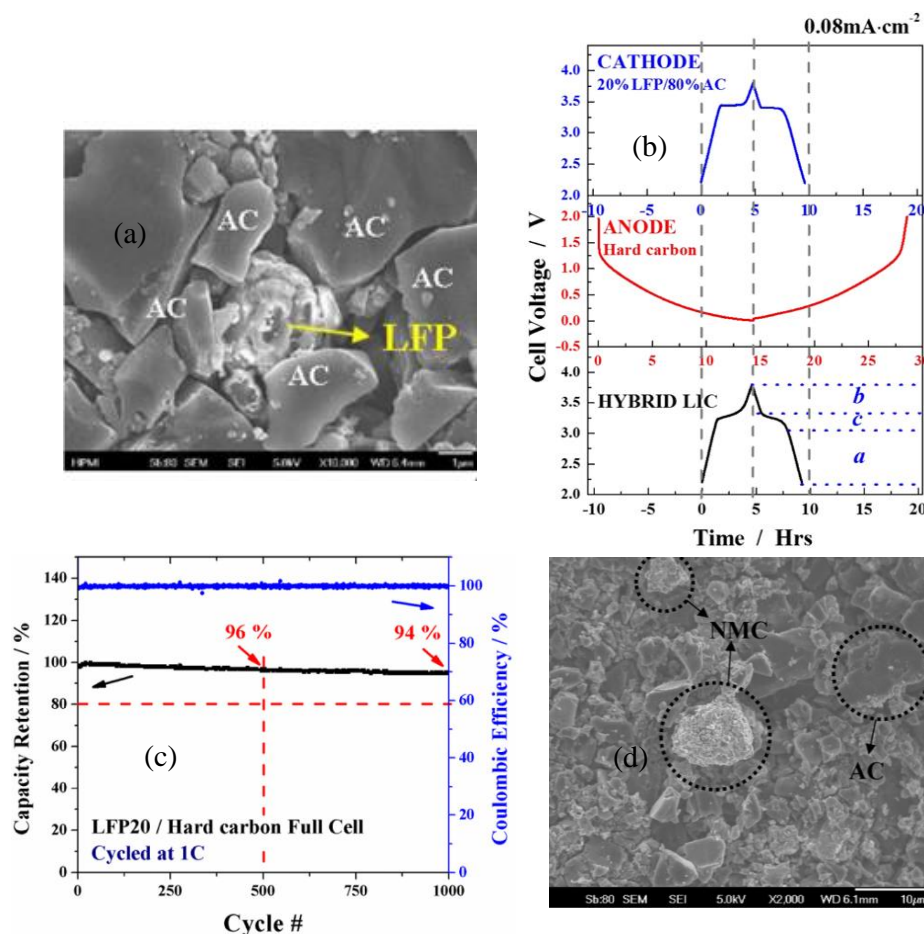
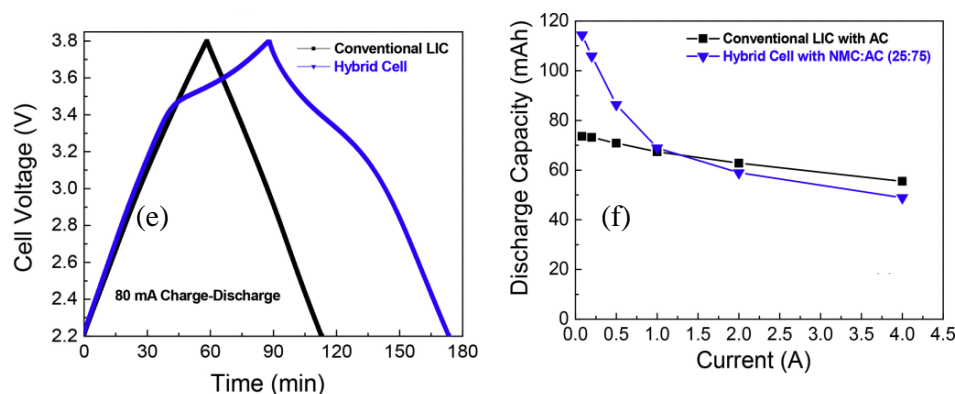


Figure 5. Cont.



**Figure 5.** (a) SEM images obtained from a hybrid LFP/AC electrode composite. (b) Capacity contribution for the individual electrodes in the hybrid cell. (c) Capacity retention of the hybrid LFP/AC LiC, retrieved from [93], copyright (2018), with permission from Elsevier. (d) SEM images obtained from the hybrid AC/NMC cell. Comparison of the (e) charge and discharge curves and (f) discharge capacity at different currents of the hybrid AC/NMC cell and conventional LiC cell, reprinted from [94], copyright (2018), with permission from Elsevier.

A capacity retention of 94% was obtained for the hybrid cathode after 1000 cycles at 1C while the pure LFP cathode realized 76% capacity retention after a similar duration. In the high C-rate cycling using 43C, a capacity retention of 76% after 20,000 cycles was obtained using the hybrid cathode; in contrast with 47% obtained by pure LFP after a similar duration. Therefore, the hybrid LFP and AC composite synergistically enhanced the energy and power density of the LiC compared to using singular AC or LFP as cathode materials. Furthermore, the beneficial effect of the hybrid cathode was more noticeable at high C-rates where the  $\text{FePO}_4$  (FP) phase plagued by low conductivity cannot be discharged entirely due to increased concentration gradient from Li salt deficiency. The AC in the composite delayed the overpotential of the LFP, improved the conductivity of the FP phase, and enhanced Li-ion transport at high current densities. Granados-Moreno et al. [95] adopted a similar bifunctional blend of AC/LFP using a 60 wt.% AC and 40 wt.% LFP composite. This composite blend achieved a specific capacity of  $102 \text{ mAh g}^{-1}$  at  $0.25 \text{ A g}^{-1}$  and  $80 \text{ mAh g}^{-1}$  at  $30 \text{ A g}^{-1}$ . A similar work using AC/LFP composites by Bockenfeld et al. [96] further highlighted the positive synergy between the AC and LFP. Diluting the LFP with the AC yielded higher specific capacity than pure LFP at high C-rates. The authors attributed to the improvement to the favorable ratio of Li-ions in the electrolyte within the pores and in the active material when the LFP was mixed with the AC. Moreover, the AC/LFP composites had improved conductivity and favorable morphology because the LFP particles, which were smaller and less porous, could occupy the spaces between the AC particles, enabling adequate contact between the two active materials. Sun et al. [97] investigated the effect of different ratios of  $\text{LiNi}_{0.5}\text{Co}_{0.2}\text{Mn}_{0.3}\text{O}_2$  (NMC) powders blended with the AC as bifunctional cathodes for LiC. A 25 wt.% NMC content was determined as the optimum blend which yielded a higher specific capacity than the pure AC ( $60.5$  vs.  $38.6 \text{ mAh g}^{-1}$ ) in the potential window 2.5–4.1 V. The hybrid AC/NMC blend enabled a 36% increase in the volumetric energy density without sacrificing the power density or cycle life compared to the pure AC cathode. Hagen et al. [94] used a similar AC/NMC (75/25 wt.%) ratio in laminate pouch cells and compared the performance to a conventional LiC using the AC as a cathode. SEM images obtained from the hybrid AC/NMC cathode are presented in Figure 5d. The NMC particles are dispersed around the AC which enables a good composite blend that would promote superior volumetric performance. The charge and discharge profiles of the conventional LiC and hybrid LiC with the AC/NMC cathode are shown in Figure 5e while the discharge capacities at various currents are compared in Figure 5f. The hybrid LiC electrode had a capacity of  $74 \text{ mAh g}^{-1}$  which was 57% higher than the capacity of the conventional AC cathode. This resulted in a 50.5% increase in specific energy. However, the power performance was marginally impacted due to the limitations of the

battery type electrode. Yu et al. [98] adopted lithium nickel cobalt aluminum oxides (NCA) as the battery-type cathode for bifunctional cathode composite blends with the AC.

The bi-functional hybrid electrode composite fabrication method can likewise affect the performance. A layer-by-layer spray printing approach was applied in developing smart multi-layer architecture electrodes incorporating dual composite materials in both the anode and cathode with an excellent energy density of  $110 \text{ Wh kg}^{-1}$  and power density of  $15 \text{ kW kg}^{-1}$  [99]. The LiC anode consisted of a spray-painted thin layer of discrete high-capacity Si (5 wt.%) at the lithium titanate (LTO) electrode surface. The same technique was applied in the cathode, which consisted of the AC and a thin spray-painted layer of LFP, but in a sandwich configuration of multi-stacked layers of spray-painted LFP and AC. The achieved high power density was enabled by optimizing the applied Si layer thickness and LFP layer thickness in the AC electrode composite sandwich. Hence, active materials with faster kinetics can be sandwiched between others with slower kinetics to improve the energy and power density.

### 3.2. Hybrid Composite with Other Carbon Materials

To achieve sufficient surface area and porosity in the synthesized AC, the precursors are often subjected to harsh gasification in the activation process, distorting the carbon structure and producing disjointed pores. Pores of varying dimensions are often created without sufficient interconnectivity when the activation methods do not include templating for tailored micropore formation. The presence of randomly created pores with insufficient interconnectivity can result in poor conductivity of the AC and inaccessibility of electrolyte ions into the pores. Moreover, while aiming to further increase the surface area, the existing micropores may collapse into mesopores and macropores from over-activation, consequentially reducing the electrode density and volumetric performance. Therefore, hybrid compositing with other carbon materials has been explored to increase the conductivity of the AC electrode and electrode density and improve the volumetric performance. Commonly incorporated carbon materials include carbon black, carbon nanotubes (CNTs), carbon nanofibers (CNFs), and carbon nanospheres (CNOs).

CNTs are widely renowned for their peculiar aspect ratios and extended graphitic layers, enabling increased conductivity and exceptional mechanical strength [100,101]. These properties facilitate improved percolation compared to typical carbon blacks when incorporated as nanotexturing composites in electrodes. Moreover, the entanglement of CNTs in the electrode composite can create open mesoporous networks, promoting the easy access of electrolyte ions to the active material. Incorporating CNTs as nanotexturing composites with the AC has yielded more superior performance than the typical carbon black often utilized [102].

CNOs in the family of carbon nanomaterials possess a very large external surface area consisting of circular stacks of carbon spheres resembling multi-walled fullerenes [103,104]. Compared to conventional carbon blacks, they possess smaller particle sizes (10 vs. 30–40 nm) and lower electrical conductivity ( $\sim 3$  vs.  $8\text{--}50 \text{ S m}^{-1}$ ) [105–107]. This smaller particle size can facilitate improved performance through easier homogenous distribution in the AC electrode, filling the interparticle voids and enhancing the conductivity. However, the ease of large aggregate formation (up to 100 nm) may present a challenge while using such materials [105].

Overall, compositing the AC with other carbon materials can result in a carbon electrode sheet with decreased interparticle void spaces. The nanoparticles filling the void spaces must be efficiently distributed with optimized percentages (2–5%) to avoid incessant agglomeration and electrode inhomogeneity. Efficiently distributed nanoparticles enable increased conductivity for the electrodes. However, a decrease in surface area with increased nanoparticles is expected. Therefore, the benefits of compositing become obvious at high current densities where the effect of electrode resistance is magnified and the capacity retention is enhanced. In contrast, no noticeable impact is expected at low current densities, and a slight decrease in capacity may occur with a reduced AC percentage in the composite.

### 3.3. Binders

Binders perform an essential role in the electrode fabrication and proper functioning of electrodes for LiC. They serve as the holding agent, securing the active materials together while simultaneously providing a conductive pathway for ionic species. The appropriate selection of binders can influence the AC electrode's mechanical strength, electrode stability, self-discharge, and ionic and electrical conductivity. Typical binders used in AC electrode fabrication include polyvinylidene difluoride (PVDF), carboxymethyl cellulose/styrene-butadiene rubber (CMC)/SBR, polytetrafluoroethylene (PTFE), polyacrylic acid (PAA), and sodium alginate. The impact of these binders on the performance of AC has been investigated by several researchers. Chen et al. [108] compared the performance of electrodes fabricated using three binders AC/PTFE, AC/PVDF, and AC/CMC/SBR, using the organic electrolyte 1M TEABF<sub>4</sub> in PC and symmetric supercapacitor configuration. It was revealed that CMC/SBR possessed the best wettability and lowest contact angle in the electrolyte. The fluoropolymers, PTFE and PVDF, had lower wettabilities due to high surface energy. Furthermore, nitrogen physisorption analysis of the AC powder and AC electrode with different binders revealed decreased porosity and surface area due to the binders. The physisorption isotherms are presented in Figure 6a. The lowest surface area was obtained from the PVDF binder while the CMC/SBR had only a minor decrease compared to the pristine AC. These microstructural differences influenced the rate performance and interfacial impedance, especially at high charge and discharge rates. The compared electrochemical impedance spectroscopy (EIS) spectra and rate performance of the different binders are presented in Figure 6b,c. The AC with CMC/SBR exhibited superior performance compared to the rest, having the lowest interfacial impedance and best capacity retention. Moreover, the CMC/SBR had the lowest self-discharge among the binders, attributed to the ease of mass transport within the macropores/mesopores favoring homogeneously adsorbed ions during charging. The homogeneously charged surface reduced the self-discharge caused by ion redistribution in the electrode.

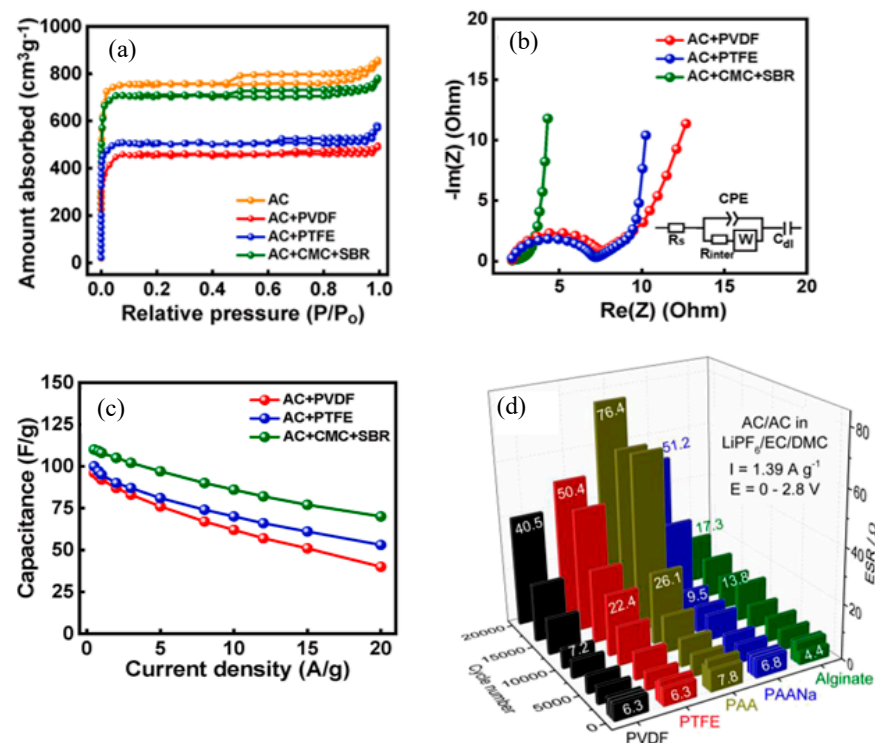


**Figure 6.** (a) N<sub>2</sub> physisorption isotherms of various samples. (b) EIS Nyquist plots, (c) Specific capacitances at various current densities for cells cycled in 1 M TEABF<sub>4</sub>/PC electrolyte, reprinted from [108], copyright (2023), with permission from Elsevier. (d) Evolution of the ESR for the corresponding cells cycling between 0 V and 2.8 V at a specific current  $I = 1.39 \text{ A g}^{-1}$  in 1 M LiPF<sub>6</sub>/EC/DMC. Reprinted from [109], copyright (2017), with permission from Elsevier.

Tran et al. [109] investigated the influence of the binders PTFE, PVDF, PAA, alginate, and PAANa (sodium polyacrylate) on the performance and cycle life of AC electrodes used in LiC. The exceptional performance of the green alginate was highlighted. Stress relaxation tests conducted during the investigation of the rheological properties revealed that the alginate based slurry remained stable whereas the PVDF/NMP slurry viscosity decreased with time. Although the authors did not disclose the reason for the unstable viscosity of the PVDF/NMP binder, we infer that certain factors related to the ability to withstand mass or phase segregation could have affected the stability of the slurry over time [110]. Since similar active materials (activated carbon) were used and the only difference was the binder, the binder interaction with the particle and ability to flocculate into larger and heavier viscoelastic masses may have caused some sedimentation, which led to a decrease in the slurry viscosity [110]. Changes in slurry viscosity are significant problems encountered while upscaling electrode slurry formulation. Hence, alginate-based binders are advantageous over typical PVDF/NMP slurries. Additionally, the water-based nature eliminates the need for adapting special process operating conditions, such as those required for PVDF while using NMP solvent. Regarding cycling performance, the alginate binder AC electrode was more stable than the PVDF. Figure 6d shows the compared equivalent series resistance (ESR) as a function of cycle number. The lowest ESR was obtained using the alginate binder. Therefore, appropriate binder selection is essential for improved electrochemical performance.

The dissolving solvents for the selected binder also play a critical role in the active material–binder interactions and the surface chemistry of the resulting electrode. Generally, electrodes could be manufactured using dissolving solvents such as water and NMP or without dissolving solvents in dry electrodes. The environmental concerns regarding using NMP have encouraged the adoption of water-based electrode formulations. In large-scale manufacturing, a solvent recovery system must be installed for NMP recovery, which increases process costs and requires high temperature for its removal. Water-based slurries, on the other hand, do not face such restrictions. However, the drying process consumes about 40% of the energy requirements in the process line [111,112]. Electrodes manufactured using the water-based process are also plagued by the changes in surface chemistry related to the oxidization of the AC upon contact with moisture. Therefore, hydrophilic groups are formed on the high surface area alongside confined moisture in the pores that are difficult to remove without extensive drying procedures. When using organic electrolytes such as the widely utilized  $\text{LiPF}_6$  salt, the tendency for hydrolysis is increased, which consequently causes the electrolyte degradation and cell capacity to fade if optimized formation procedures are not conducted.

Moreover, lots of gas generation is expected during the formation step as the electrolyte hydrolysis reactions are accelerated. On the contrary, the surface of the AC electrode with NMP is more hydrophobic; issues regarding confined moisture in the pores are minimal. However, NMP has a high boiling point of 202 °C [111] which means that some of the NMP may remain in the AC pores if extensive drying procedures are not incorporated. Remnant solvents in the pores can cause increased pressure buildup in cells since they diffuse and affect the device's operation. Given these limitations, dry electrodes involving no dispersing solvents are promising alternatives that eliminate drying and solvent recovery costs. Moreover, the dry electrode method can enable the realization of high areal capacity electrodes which are often difficult to attain using the slurry methods due to viscosity and flowability issues. Furthermore, the hydrophobic surface chemistry inherited from the polymer binder is preserved and the surface chemistry remains unmodified without any solvent, thus improving the wettability in organic electrolytes.

#### 4. Electrolyte Optimization

Electrolytes are indispensable components in energy storage devices. Electrolytes enable the operation of energy storage devices by performing diverse roles, such as facilitating ion transfer between cathodes and anodes, stabilizing electrode surfaces, and

promoting electrochemical stability and device performance [113,114]. The electrolytes used in LiC consist of a salt of the corresponding metal ion dissolved in a solvent or solvent combination, with or without additives. These electrolyte constituents are optimized to influence the conductivity, viscosity, density, operating potential window, and operating temperature. Factors such as the metal ion transport between the cathode and anode, cathode and anode interfacial stability, device cycle life, energy, and power density are hence affected by the nature of the electrolyte.

#### 4.1. Electrolyte Solvents

Electrolyte solvents dissolve the electrolyte salt to enable dissociation into mobile conducting ions enclosed by a solvation shell. The nature of the dissolving solvent affects the electrolyte classification, which could be aqueous or nonaqueous, an ionic liquid, or solid-state electrolytes without any dissolving liquid solvent. The latter two are not widely applied in LiC due to the rigorous preparation conditions, high costs for the ionic liquids, and poor conductivity of the solid-state polymer electrolytes at low temperatures. Meanwhile, the aqueous electrolytes are limited by the decomposition potential of water at 1.2 V which restricts the operating potential window. Even though very high conductivity and high capacitances can be obtained using such electrolytes, the resulting energy density remains constrained due to the low operating potential window. Nonaqueous electrolytes, on the other hand, yield lower capacitance from the bulkier solvated ions dimensions but higher energy densities due to the wider operating potential window. Hence, the solvent choice can significantly affect the performance of the device. Additionally, other benefits such as the formation of ternary graphite intercalation compounds in graphite anodes used in sodium-ion capacitors have been achieved through optimized glyme-solvated electrolytes [115]. In the absence of such ternary graphite compounds, the binary counterparts would intercalate between the graphene layers, thereby resulting in exfoliation, instability, and, consequently, negligible energy storage capacity in the graphite anode.

Among the nonaqueous electrolytes, carbonate solvent-based electrolytes are widely adopted in LiC due to their ability to operate at higher maximum potentials (>4 V) compared to conventional supercapacitor solvents such as acetonitrile (~2.7 V). The latter solvent is unstable at potentials below 0.5 V vs. Li but possesses higher conductivity and superior low-temperature performance than the former. However, the ion-solvent interaction can influence the AC's rate performance, especially at high C-rates. Carbonate solvents, such as EC, possess significantly larger dipole moments and bind more strongly to the Li cation than acetonitrile. Therefore, the strong coordination of EC to Li impacts the difficulty in the desolvation process by the surrounding electric field. This can interfere with the specific capacitance at high C-rates since the optimum pore size for the maximum power density is affected. The pore size of the AC must accommodate the dimensions of the solvated ion and allow for free diffusion of charges without affecting the double layer. Decaux et al. [116] investigated the influence of these two solvents on the performance of AC electrodes. It was revealed that larger pore dimensions in the range of 1.1 to 1.3 nm are needed to achieve increased capacity when using carbonate solvents. On the contrary, the easily de-solvated acetonitrile solvent required smaller pore dimensions (0.7–0.8 nm) to achieve the maximum specific capacitance.

Although high conductivity in electrolytes is required for high-power and high-rate cycling, the electrochemical stability at the electrode surface is equally important. Surface functionalities introduced deliberately or inadvertently during the AC production can affect the electrochemical stability.

The choice of solvent can also promote ion adsorption on the AC surface by optimizing the initial electrode potential. ho Lee et al. [117] reported on the effect of tetrahydrofuran (THF) on the AC capacity. The authors showed that adding THF to the electrolyte (1M LiBF<sub>4</sub> in EC:DEC(3:7)vol%) resulted in a shift in the electrolyte electrostatic potential, increased ionic mobility, and easier adsorption of the BF<sub>4</sub> anion on the AC electrode surface. ho Lee et al. [118] also reported enhanced rate performance of an AC/Li LiC

achieved via the addition of 1,3,5-trifluoro benzene (TFB) in the electrolyte (1M LiBF<sub>4</sub> in EC:DEC(3:7)vol%).

The electrochemical stability of the chosen solvent can influence the stability of the electrolytes. Aqueous solvents are limited by the decomposition of water at 1.2 V, which causes severe gas evolutions when operating at these limits. On the contrary, organic solvents typically operate at wider potential windows and have varying oxidative and reductive stabilities depending on the solvent or solvent combinations. The oxidative and reductive stability of the solvents can be estimated from the density functional theory calculations of their respective highest occupied molecular orbital (HUMO), lowest unoccupied molecular orbital (LUMO), and experimental examinations using typical inert working electrodes like glassy carbon or platinum [119]. However, the actual stability on the carbonaceous AC electrode differs from such experiments due to the carbon electrode/electrolyte interactions which limit the operating potential window and stability following oxidation of the surface at high potentials. Since similar LiB electrolytes are used in LiC, various researchers have investigated the oxidative and reductive stabilities of different electrolyte solvents and solvent combinations [113,120,121]. Carbonate solvents such as cyclic and linear carbonates like ethylene carbonate (EC), propylene carbonate (PC), ethyl methyl carbonate (EMC), dimethyl carbonate (DMC), and di ethyl carbonate (DEC) are usually the preferred alternatives due to the relatively higher operating potential windows and the ability to form passivation films on the negative electrode. However, these solvents typically decompose on the high surface area of the AC and such reactions are exacerbated by surface oxygen functionalities and confined moisture in the pores [122]. The decomposition products affect the morphology of the AC and reduce the available surface area and pores for the charge storage [123]. Other solvent types, such as the sulfonated derivatives, sulfone, and dimethyl sulfide have been reported to exhibit higher oxidative stabilities than the carbonate solvents [114]. However, these classes of solvents typically have higher viscosities and necessitate mixtures with low-viscosity solvents to maximize the operating temperature window. Recently, very promising fluorinated solvents have demonstrated excellent oxidative and reductive stabilities due to the strong electronegativity of fluorine that influences the LUMO and HUMO [124,125]. Therefore, they exhibit higher oxidation stabilities than typical carbonate solvents and can form fluorine-rich and stable interfaces on the negative electrolyte that synergistically enhance the cycle life [125].

#### 4.2. Electrolyte Salts

Several metal-ion salts have been investigated with different degrees of dissociating ability, capacity, and conductivity in carbonate solvent blends. Using Li-salts as an example, LiPF<sub>6</sub>, LiTFSI, LiFSI, LiCF<sub>3</sub>SO<sub>3</sub>, LiClO<sub>4</sub>, and LiBF<sub>4</sub> are some notable examples that have been explored. Amatucci et al. [3] emphasized the importance of optimizing the electrolyte salt capacity and molecular weight in hybrid ion capacitors. The electrolyte salts LiPF<sub>6</sub>, LiCF<sub>3</sub>SO<sub>3</sub>, LiClO<sub>4</sub>, and LiBF<sub>4</sub> were revealed to possess capacities of 176, 272, 252, and 286 mAh g<sup>-1</sup>, respectively. Moreover, using electrolyte salts with a high molecular weight could decrease the energy density of the LiC. Furthermore, the anions, in particular, influence the obtainable capacity of the AC electrode. The variation in electrochemical performance of the AC electrode using different lithium salts in the electrolyte can also be correlated with the dimension of the de-solvated anions (Figure 7a). Kato et al. [126] examined the influence of Li-salts with various anions on the performance of AC/LTO LiC. The rate performance of the different electrolytes is presented in Figure 7b. As expected, the Li-salt with the largest de-solvated anion dimension had the lowest capacity. However, LiBF<sub>4</sub>, with the smallest de-solvated anion dimension, did not possess the largest specific capacity. The authors emphasized that the discrepancy was due to the lower conductivity of the LiBF<sub>4</sub> electrolyte which was attributed to the lower dissociation constant observed for the BF<sub>4</sub><sup>-</sup> anion compared to the others. Therefore, the importance of selecting appropriate electrolyte salts with de-solvated anion dimensions suited to the AC pores and an optimum balance in conductivity is further demonstrated.

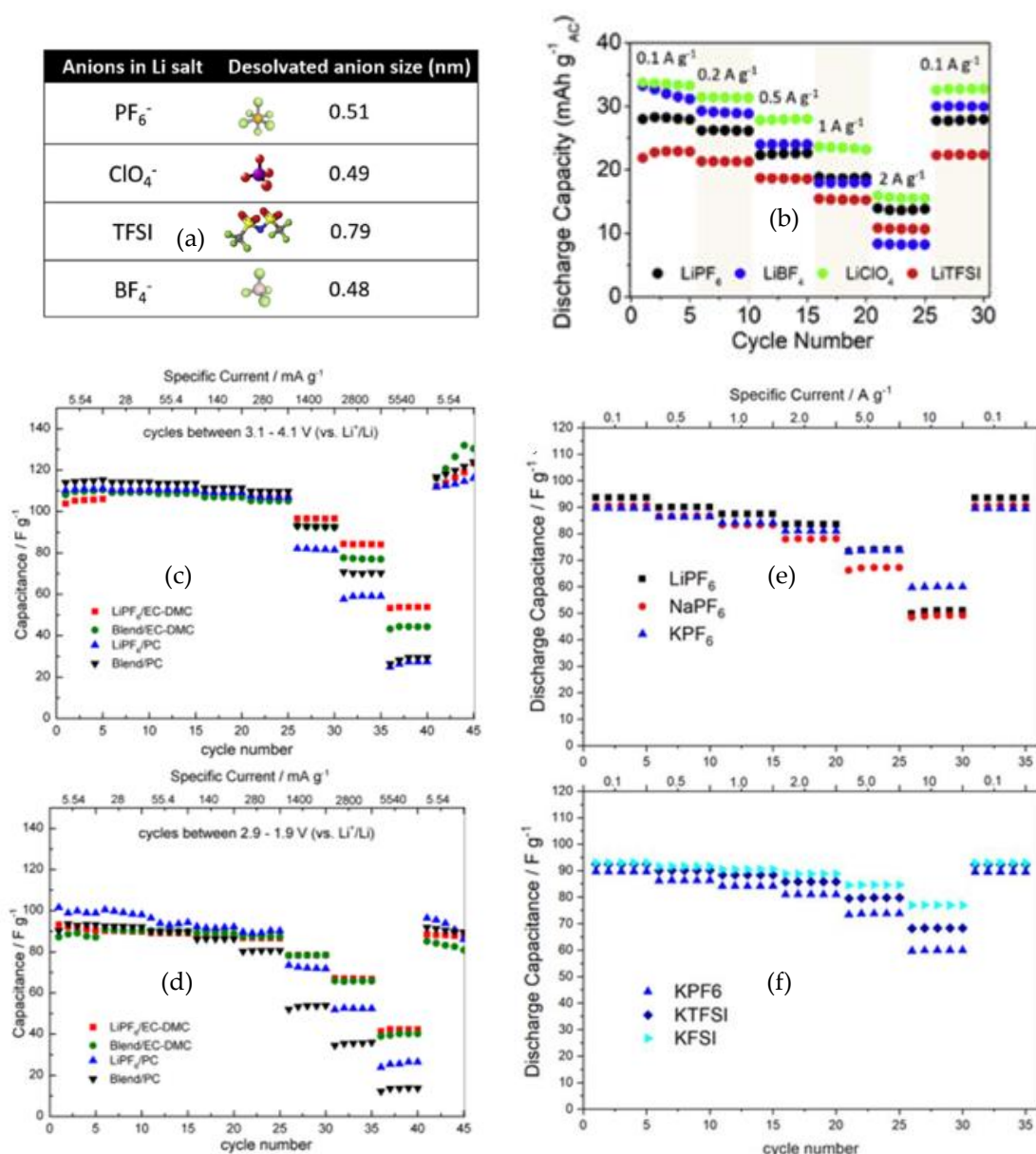


**Figure 7.** (a) De-solvated anion sizes and structures of some lithium salts. (b) Rate performance comparison of the different electrolytes, reprinted from [126], copyright (2019), with permission from Elsevier. Gravimetric specific capacitance of AC electrodes in different electrolytes. (c) Electrodes cycled between 3.1 V and 4.1 V vs. Li<sup>+</sup>/Li. (d) Electrodes cycled between 2.9 V and 1.9 V vs. Li<sup>+</sup>/Li, reprinted from [120], copyright (2016), with permission from Elsevier. (e,f) Rate capabilities of symmetric AC//AC capacitor cells in different electrolytes, reprinted from [127] (CC-BY).

Researchers have implemented dual anion salts to maximize the available capacity through the adsorption of ions of various dimensions. In a notable work, Zhang et al. [120] investigated the electrochemical performance of electrolyte salt blends consisting of  $\text{NET}_4\text{BF}_4$  and  $\text{LiPF}_6$  dissolved in singular PC or EC:DMC (1:1) compared to singular  $\text{LiPF}_6$  or  $\text{LiBF}_4$ .  $\text{LiBF}_4$  exhibited inferior performance due to the highest equivalent series resistance and lowest conductivity, necessitating the substitution with  $\text{NET}_4\text{BF}_4$ . The rate performance of the electrolytes in different potential windows covering anion and cation utilization is displayed in Figure 7c,d. It was interesting to observe that the capacitance of the electrolyte blend ( $\text{NET}_4\text{BF}_4$  and  $\text{LiPF}_6$ ) was higher than the singular  $\text{LiPF}_6$  at low current densities. However, at high current densities, the opposite occurred. This may have been caused

by increased competition between the dual anions at the AC pore entrance, creating a sieving effect and consequentially slightly lower capacity than singular  $\text{LiPF}_6$ . Moreover, the solvation shell contributed by the dissolving solvent also affected the performance and electrochemical stability.

The various alkali metal salts (derivatives of Li, Na, and K) possess different stabilities and distinct electrochemical performances when used as electrolyte salts with the same AC and organic solvents. Stpie et al. [127] investigated the electrochemical behavior of AC when exposed to different electrolytes based on Li, Na, and K salts containing the anions ( $\text{PF}_6$ , FSI, and TFSI) in similar solvents. The rate performance of the compared cations is presented in Figure 7e while the anions comparison with K is presented in Figure 7f. It was revealed that electrolytes based on the K-salts exhibited superior performance with higher ionic conductivity and faster ion diffusion within the AC micropores. Moreover, the larger K cation and “softer” character compared to Li facilitated less interaction with the electrolyte decomposition active sites on the AC and displayed a lower desolvation energy. Meanwhile, the strong acidic character of Li and binding energy to the solvent caused the increased presence of solvents in the AC pores where most decomposition reactions occur. The ease of desolvation of the K cation reduces the amount of solvent in the pores; thus, solvent decomposition occurs mostly at the external surface.

#### 4.3. Electrolyte Dielectric and Viscosity

Properties of the electrolytes, such as dielectric, viscosity, and conductivity, have also been demonstrated to affect the self-discharge, rate performance, and electrochemical stability of the AC cathode. Eleri et al. [128] revealed that the electrolyte dielectric can influence the electrochemical stability of the AC cathode. Increasing the electrolyte dielectric improved the anion oxidative stability at the double layer region by modifying the solvation shell and increasing the resistance to oxidation during polarization at high energies. However, the increased dielectric leads to increased solvation energies and high viscosity [129,130]. Moreover, increased solvation energy results in high charge transfer resistance at the anodes due to high activation energy for desolvation, impacting the rate performance at high current densities [129,131]. Nevertheless, the cycling stability and coulombic efficiency of the cells with high dielectric solutions are superior to low dielectric electrolytes. The impacted rate performance at high current densities using high dielectric electrolytes could be mitigated by adequately tuning the AC pore size to enable the optimum adsorption of solvated and de-solvated ions and sufficient mass balancing on the anode.

Although a high dielectric is needed to achieve adequate salt dissociation, low dielectric electrolytes have also been optimized to reduce the solvation energies and improve the dissociation rate and conductivity through dual-cation systems. Chikaoka et al. [132] achieved a very high power density and improved stability in an AC/LTO LiC by using a dual-cation low-dielectric electrolyte. The electrolyte consisted of a mixture of spiro-(1,1)-bipyrrolidinium tetrafluoroborate ( $\text{SBPBF}_4$ ) and  $\text{LiBF}_4$  dissolved in DMC. The dual cation system eliminated the phase separation behavior and ion pairs caused by the single cation dissolution in the low dielectric DMC. Therefore, the low dielectric dual cation electrolyte had improved power density due to the low viscosity and improved conductivity.

## 5. Cell Design Optimization

The hybrid nature of LiC necessitates meticulous design to counter the imbalance of the capacitive AC cathode and the energy-dense intercalation type anode. The imbalance is due to the sluggish kinetics of the anode, in contrast with the rapid charge storage by ion physisorption occurring on the AC cathode. Consequentially, inadequate cell design can present issues such as underutilized potential windows, electrode potential encroachment into unsafe electrolyte decomposition regions, poor cycle life, and limited energy and power density. The following section discusses recent cell design strategies to improve the performance of the AC.

### 5.1. Capacity Balancing

Capacity balancing is a fundamental step required for the optimum performance of LiC due to the mismatch between the capacity of the AC cathode and the significantly larger anode material. High-power symmetric SC utilizes a 1:1 direct cathode: anode balance, which guarantees high power along with the rapid physisorption kinetics of the AC material [133,134]. However, if such ratios are utilized in LiC, for example, using the AC cathode (specific capacity  $<60 \text{ mAh g}^{-1}$ ) and the HC anode (specific capacity  $>360 \text{ mAh g}^{-1}$ ), the AC capacity would be completely charged before the anode. Moreover, the energy density is reduced since the anode potential is underutilized and may swing toward unstable regions where electrolyte degradation is accelerated [135].

It has been demonstrated in several works that a cathode:anode mass ratio  $>4$  is required to achieve very high energy density in LiC [8,136]. Using such high mass ratios enables complete utilization of the anode capacity since an equal charge balance can be achieved between the AC cathode and the battery-type anode, improving the device capacity and energy density. Dsoke et al. [136] explicitly highlight the effect of the electrode mass ratio on the performance of AC/LTO LiC. The authors compared the performance of LiC of different electrode mass ratios, starting from the classically balanced mass ratio of 4.17:1 derived from the experimentally obtained AC electrode capacity of  $38.36 \text{ mAh g}^{-1}$  and LTO electrode capacity of  $160 \text{ mAh g}^{-1}$ . Therefore, the AC electrode thickness was increased to 4.17 times the initial mass while the LTO mass was kept constant. The schematics of the cells are presented in Figure 8a. Figure 8b,c shows the capacity retention and Ragone plots of AC/LTO LiCs assembled with different mass ratios and a symmetric AC/AC supercapacitor cell for comparison.

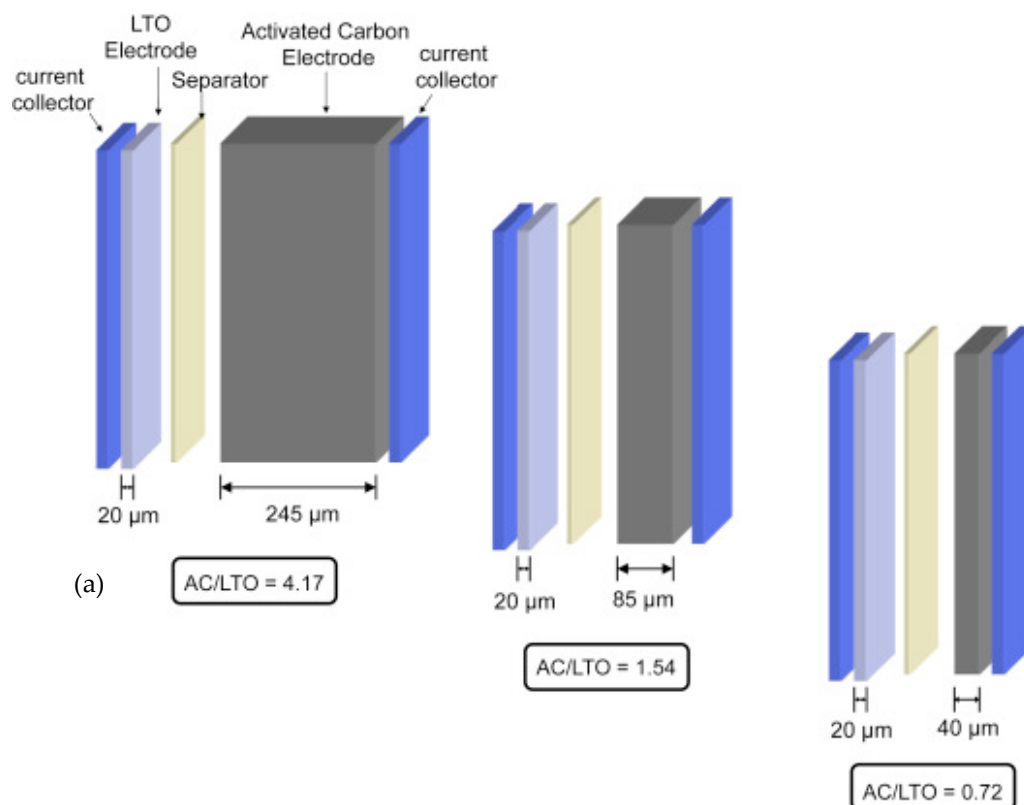
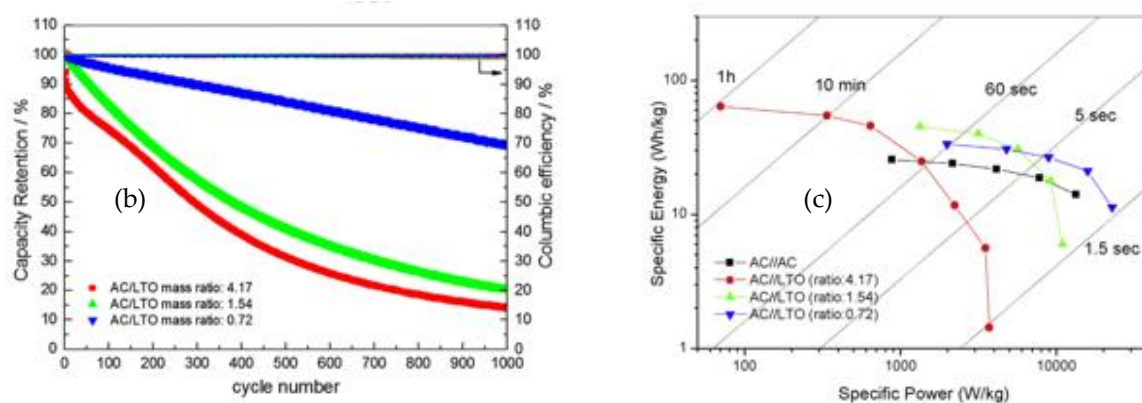


Figure 8. Cont.



**Figure 8.** (a) Schematic of AC/LTO systems balanced with an AC/LTO mass ratio of 4.17, 1.54, and 0.72. (b) Capacity retention of the cells after 1000 cycles at 10C. (c) Ragone plots of AC/LTO LiC assembled with different mass ratios. Reprinted from [136], copyright (2015), with permission from Elsevier.

As the AC/LTO mass ratio increased, the energy density increased while the capacity retention decreased. It is worth noting that the cycle life of LiC with a very high energy density deteriorates faster when such high mass ratios are utilized to achieve a similar capacity as the LiB counterparts. Moreover, the overall energy density of the cell is also significantly reduced after accounting for the weight of active materials which are mostly subjected to weight and thickness constraints.

### 5.2. Operating Potential Window Regulation

The operating potential window influences the capacity, electrode stability, and achievable energy and power density. Operating beyond stable limits can lead to encroachment into regions where electrolyte decomposition may be accelerated at the upper or lower vertex potentials. Furthermore, the anodes deliver distinct electrochemical performance depending on the potential window [137]. Therefore, investigating the operating potential window of the AC and selecting appropriate regions on the anode where kinetics mismatch can be alleviated is necessary. Jin et al. [137] demonstrated a practical matching approach for selecting an appropriate potential region during the design and fabrication of an AC/HC LiC. The authors first determined the appropriate operating potential region of the HC anode using a combination of galvanostatic charge and discharge analysis (GCD), galvanostatic intermittent titration technique (GITT), and electrochemical impedance spectroscopy (EIS) conducted at different potentials to observe the corresponding distinct electrochemical processes. After evaluating the appropriate region, the HC anode was pre-lithiated to enable operation within the chosen region and matched with the appropriate mass balance to the AC cathode and working potential. Incorporating these processes improved the energy density, power density, and life cycle.

Several operating potential limits for the AC cathodes have been utilized in various research, ranging from 1.5 to 4.6 V. Increasing the operating potential window enhances the capacity until a trade-off at these limits where further increased potential does not correspond to increased capacity. Moreover, electrolyte decomposition is accelerated at these limits and accompanied by severe passivation of the AC electrode surface by electrolyte decomposition products. The cycling stability is also affected by faradaic processes whose magnitude may vary based on the chosen potential window. Zhang et al. [138] investigated the capacity retention of AC/HC LiC cycled in different potential windows, namely 2.0–4.0 V and 2.2–3.8 V. The capacity retention was 73.8% after 80,000 cycles in the former and 94.5% of the initial value after 200,000 cycles in the latter. The selection of safe operating potential windows depends on the evaluation method, an objective widely explored by various researchers [139,140]. Sun et al. [141] reported a method for determining the operating potential of the AC cathode without the influence of the anode. The authors

established that the stable potential limits can be obtained using the energy efficiency and the criterion that the second derivative of the  $S$  value plotted against the vertex potential,  $d^2S/dU^2 < 0.05$ . The operating potential limit of the AC in their study was determined to be 2.2–3.9 V. However, these operating potential limits depend on the nature of the electrolyte (organic solvent and salt) and operating temperature. Other parameters such as the presence of oxygenated functional groups on the AC surface, binder type (CMC/SBR vs. PTFE), and aluminum current collector (etched vs. carbon coated) can significantly influence the operating potential window of the AC. Compared to the alternatives, superior stabilities are obtained using coated collectors and PTFE binders [141].

Although the AC-specific capacity can be increased by utilizing more expansive potential windows, the oxidative stability is adversely affected at too high potentials. At the same time, the reversibility is impacted at low potentials. The impacted oxidative stability is associated with the oxygen functionalities discussed earlier that are responsible for increased capacitance through pseudocapacitance but impact cycling stabilities. Zhang et al. [142] deduced the following mechanism via which the oxidative stability is affected by oxygen functionalities when operating at high potentials. When the AC electrode is cycled at high potentials, the oxygen functionalities likely present in the form of ketones, ethers, lactones, carboxyls, etc., and are oxidized at such high potentials to form  $\text{CO}_2$  and  $\text{H}_2\text{O}$ . The  $\text{H}_2\text{O}$  hydrolyses the  $\text{LiPF}_6$  salt and further reacts with the lithiated negative electrode to form  $\text{Li}_2\text{O}$  and  $\text{H}_2$ . Therefore, large amounts of gases are generated together with the detrimental HF that causes interfacial instabilities and further depletes the active  $\text{Li}^+$  ions. At lower potentials, increased  $\text{Li}^+$  trapping occurs on the micropores due to the poor Li reversibility caused by the reactions with oxygen functionalities on the AC. These limitations have consequently led to manufacturers adopting the operating potential window 2.2–3.8 V as the recommended limit in dual carbon LiC, whereby appreciable capacity is maintained without compromising the cycling stability of the cell. By retaining this limit, oxidation reactions on the AC surface and lithium trapping at too low potentials by the reduced surface functionalities are minimized.

### 5.3. Pre-Lithiation

In contrast with the battery counterparts, LiC possesses no metal-ion source other than the metal ions in the electrolyte. However, during the initial cycling process, the formation of SEI on the anode and cathode can rapidly deplete the already-limited metal ions in the cell. Therefore, a pre-lithiation step is necessary to increase the availability of metal ions for charge storage. The pre-lithiation also mitigates against metal-ion depletion after the SEI formation on the anodes, resulting in enhanced cycling performance without a change in the materials or device structure [143]. Moreover, sufficient metal ions allow the AC cathode to operate at a widened potential window through the adsorption of metal cations below the OCP and anions above the OCP. As a result, the capacity of the AC cathode is increased and the resulting energy density for the LiC is enhanced. Pre-lithiation also facilitates safe anode utilization within the typical electrolyte decomposition limits  $< 0.8$  V by forming an initial SEI with the excess metal ions.

The process of pre-lithiation is commonly achieved using various electrochemical or direct contact pre-metalation techniques [143,144]. Central to each method is a sacrificial metal cation source where cations migrate from and to the anode either under the influence of an externally applied electrochemical driving force or by internal or external short-circuiting after direct contact. The pre-lithiation step could also be conducted as a pre-assembly procedure where the anode is pre-cycled with the metal cation source and the potential is regulated to the desired pre-lithiation degree before disassembly and reassembly of the final full cell with the intended cathode. In this case, two cell assembly steps are needed, which may complicate assembly line procedure in full-scale manufacturing and present additional contamination risks. Moreover, the direct contact method is usually conducted with the corresponding pure metal as the metal cation source. Consequently, the direct contact method is often uncontrollable, with a nonuniform degree of pre-lithiation

since the strategy relies on direct contact between the metal and anode with no external controlling force. Moreover, the risk of thermal runways, fire hazards, and others associated with handling the highly reactive pure metal is significant and may pose serious concerns during large-scale assembly.

In response to the above concerns, a new pre-lithiation technique was developed which involves incorporating inorganic or organic sacrificial compounds containing the metal cations as an alternative to using the highly reactive pure metal during pre-lithiation [144–146]. These sacrificial compounds are composited in the AC cathode during the electrode fabrication process. The selection of sacrificial cathode pre-lithiation additives is based on the ability to irreversibly de-lithiate in the working potential window of the cathode and exhibit high volumetric or gravimetric capacity while remaining electrochemically, chemically, and thermally stable under electrode processing conditions and after the de-lithiation. Examples of such additives include  $\text{Li}_2\text{MoO}_3$  [147],  $\text{Li}_5\text{FeO}_4$  [148],  $\text{Li}_2\text{DHBN}$  [149],  $\text{Li}_3\text{N}$  [150],  $\text{Na}_2\text{S}$  [151],  $\text{NaCN}$  [152],  $\text{NaNH}_2$  [153],  $\text{Na}_2\text{C}_4\text{O}_4$  [154],  $\text{Li}_2\text{C}_4\text{O}_4$  [146], and  $\text{Li}_2\text{C}_4\text{O}_6$  [155].

Park et al. [147,148] used  $\text{Li}_2\text{MoO}_3$  and  $\text{Li}_5\text{FeO}_4$  as sacrificial pre-lithiation additives mixed with the AC electrode during the fabrication of LiC. However, the oxidation of these materials occurred at high potentials (4.7 V) which are in regions where electrolyte oxidation is prominent; the AC surface can easily be passivated at the detriment of the surface charge storage capacity. Moreover, there is a remnant inactive mass in the cell which subsequently decreases the specific energy of the LiC. The sacrificial salts, therefore, show more promise because they produce no residues after de-metalation. The listed ternary salts only produce  $\text{N}_2$  and  $\text{CO}_2$  gases which can be removed during the formation step. This is particularly important when using capacitive materials since any residue after the de-lithiation can block the pores or contribute to inactive masses in the cell. Arnaiz et al. [146] demonstrated an effective pre-metalation strategy using  $\text{Li}_2\text{C}_4\text{O}_4$  and the K and Na derivatives as sacrificial pre-metalation additives mixed with the AC cathode and paired with an HC anode. Cyclic voltammetry (CV) and galvanostatic charge and discharge analysis conducted on the composite  $\text{Li}_2\text{C}_4\text{O}_4$ , conductive additive, and binder (65:30:5 mass ratio) are presented in Figure 9a,b. The results revealed the irreversible capacity ( $375 \text{ mAh g}^{-1}$ ) provided by the composite during the first cycle, as further evidenced by the broad peaks which diminished severely in subsequent cycles. Hence, confirming that the  $\text{Li}_2\text{C}_4\text{O}_4$  is able to irreversibly oxidize in the first cycle and is completely consumed after the 10th cycle. The AC/ $\text{Li}_2\text{C}_4\text{O}_4$  composite CV curves are displayed in Figure 9c. Similar first-cycle broad peaks are observed, attributed to the irreversible oxidation of the  $\text{Li}_2\text{C}_4\text{O}_4$ . These broad peaks were absent in the 10th cycle, with the CV profile exhibiting the typical regular box-like characteristics of the AC.

Furthermore, it was revealed in this work that the pre-lithiation process did not affect the performance of the AC. On the contrary, the rate performance of the recovered AC after the de-lithiation of the  $\text{Li}_2\text{C}_4\text{O}_4$  agent was superior to the AC without the pre-lithiation, as shown in Figure 9d. Post-mortem electrode examinations revealed void spaces in the AC after the pre-lithiation attributed to the oxidation of  $\text{Li}_2\text{C}_4\text{O}_4$  in the electrode. The cycled pre-lithiated electrode further exhibited microstructural changes, evidenced by the creation of additional meso and macroporosity in the AC. These microstructural changes on the AC electrode were beneficial for improved electrolyte accessibility and superior rate performance.

Although the sacrificial salts show more promise, it is desirable in production lines to avoid extra gas formation after the pre-lithiation process. Recently, Pan et al. [152] effectively pre-sodiated the anode in a sodium ion capacitor by mixing the AC cathode with sodium cyanide (NaCN) as a pre-sodiation additive. The oxidation of the NaCN occurred at 2.9 V vs.  $\text{Na}/\text{Na}^+$  with a capacity of  $547 \text{ mAh g}^{-1}$  without any gas evolution.

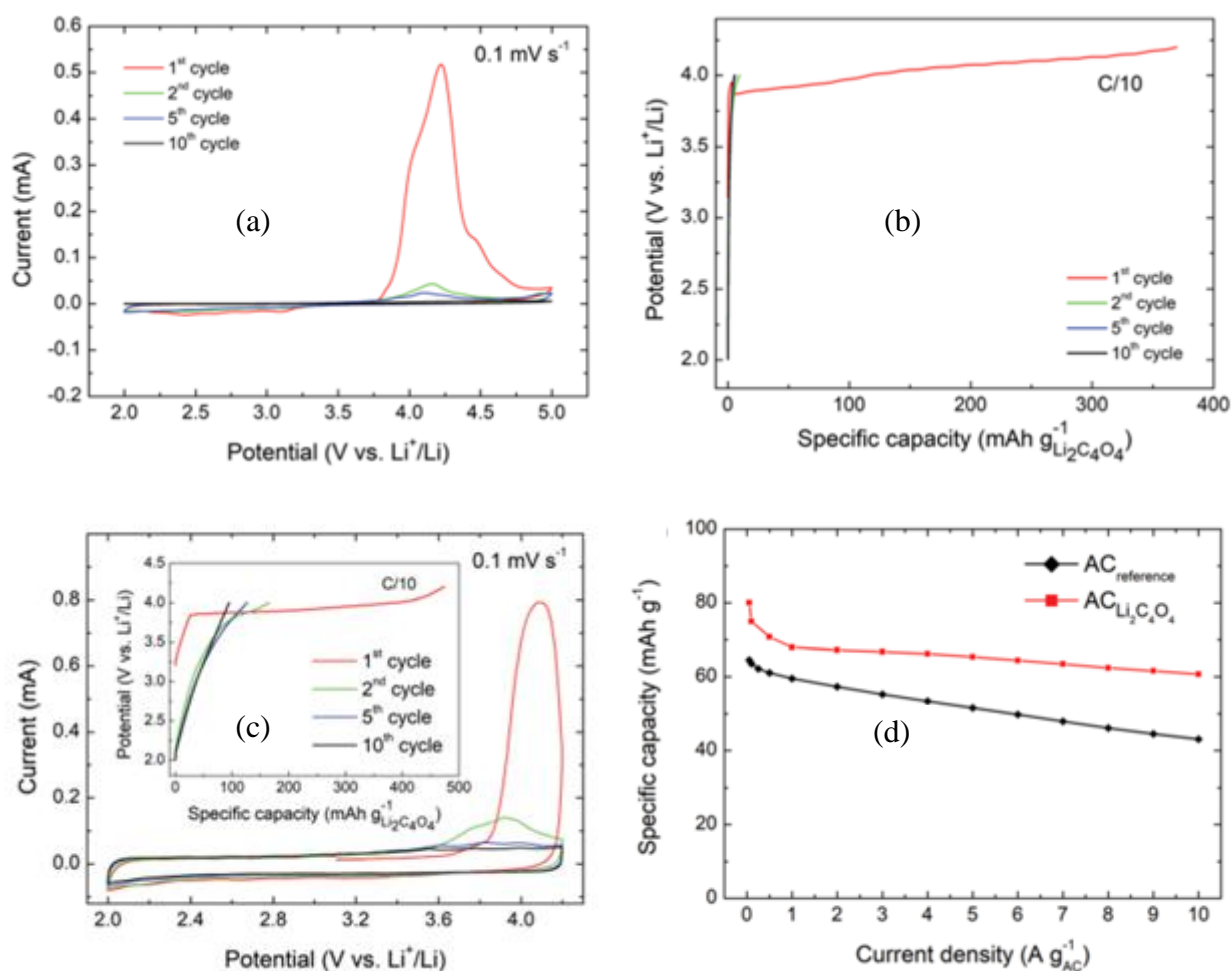


**Figure 9.** Electrochemical characterization of the as-prepared  $\text{Li}_2\text{C}_4\text{O}_4$  salt mixed with conductive carbon and binder in a 65:30:5 mass ratio. (a) Cyclic voltammetry (CV) at  $0.1 \text{ mV s}^{-1}$  and (b) galvanostatic charges at C/10. Electrochemical characterization of the as-prepared  $\text{AC}_{\text{Li}_2\text{C}_4\text{O}_4}$  electrode: (c) CV at  $0.1 \text{ mV s}^{-1}$ , inset: galvanostatic charge at C/10, and (d) specific capacity values at different current densities for the  $\text{AC}_{\text{Li}_2\text{C}_4\text{O}_4}$  and the  $\text{AC}_{\text{reference}}$  electrodes. Retrieved from [146], copyright (2020), with permission from Royal Society of Chemistry (RSC).

Some sacrificial pre-lithiation additives can serve as dual-functioning additives to pre-metalate the anode while increasing the capacitance of the AC through pseudocapacitance. Zhang et al. [156] demonstrated the use of Li-rich  $\text{Li}_2\text{CuO}_2$  as a cathode prelithiation additive during the fabrication of AC/graphite LiC. The AC/ $\text{Li}_2\text{CuO}_2$  cathode composite was revealed to behave as a pure capacitor when cycled between 2.8 and 4.2 V, yielding similar capacitance and capacity as the AC/Li half-cell. However, when the operating potential window was changed to 2.0–4.0 V, the remnant  $\text{Li}_2\text{CuO}_2$  provided extra capacitance through pseudocapacitive behavior (increased from  $150 \text{ F g}^{-1}$  to  $189 \text{ F g}^{-1}$ ) after irreversible delithiation in the first cycle ( $342 \text{ mAh g}^{-1}$ ).

## 6. Outlook and Perspectives

Different strategies enabling the increased performance of the AC cathode, when used in LiC, have been discussed. These strategies encompassed material, electrode, electrolyte, and cell design optimization techniques which enabled increased capacity, operating potential window, and stability of the AC cathode. Among the precursors, self-activating precursors present an opportunity to create high-performance AC with optimized pore size distribution by a simple controlled carbonization step. However, they

are often plagued by heterogeneously distributed concentrations of atomically dispersed alkali metals. We propose an approach adapted from the self-activating biomass precursors whereby synthetic precursors are developed with nanoscale/atomically dispersed alkali metals. Using such synthetic precursors and controlled percentages of the dispersed alkali metals will enable the production of high-quality AC with controlled pore size distribution and high purity.

Introducing some degree of graphitization in the AC presents another approach for enhancing the capacity. However, care should be taken to optimize the graphitization degree to improve the capacity without affecting the rate performance. The implementation of this technique will enable a hybrid charge storage mechanism consisting of shallow intercalation and the typical ion adsorption/desorption in the AC pores.

The beneficial effects of functionalization, particularly the oxygen functional groups, were demonstrated by many studies. Oxygen functionalization can be beneficial and likewise detrimental to the performance. However, a critical understanding of these redox processes occurring on the electrode surface following reactions with the electrolyte at different potentials is needed. This could be achieved via *in situ* studies by analyzing reaction products generated during electrochemical cycling and relating such products with the performance of the AC.

On the electrode level, compositing with bi-functional electrodes presents a rational strategy to improve the AC's capacity but with slight decrease in the rate performance. However, nanostructuring during active material synthesis can improve the rate performance of the composites. The high-capacity battery-type cathode could be nanosized and coated with a carbon precursor, which can later be activated. Hence, creating a bi-functional active material consisting of an inner core of high-capacity battery-type cathode and an outer shell of AC will enhance the charge storage kinetics.

Lastly, a fundamental understanding of the AC and battery-type electrode interaction is lacking, especially at the electrode–electrolyte interface. The influence of chemical cross-talks between the reaction by-products formed after reactions between the AC surface functionalities and the electrolyte needs to be investigated. These by-products can possibly migrate to the battery-type anode and negatively affect the SEI properties. Similarly, the SEI film forming additives introduced to influence the anode SEI may likewise affect the AC performance due to chemical cross-talks. Although it is widely accepted that the AC stores charge through ion adsorption in the double layer, the passivation film forming abilities of carbonate solvents may alter the performance. Hence, the broad question is whether the AC electrode–electrolyte interface can be influenced by film forming additives to delay electrolyte degradation or increase the operating potential window. If so, the consequences of such film-forming additives on the capacity/capacitance and the effect on the charge storage mechanism need to be understood.

In this review, we have outlined several strategies by which the performance of the AC cathode can be enhanced beyond the typical activation method optimization. These techniques mentioned, together with the future research directions, can facilitate improved performance of the AC cathode and subsequential energy and power density of the LiC.

**Author Contributions:** O.E.E.: Conceptualization, Data Curation, Investigation, Methodology, Visualization, Writing—Original draft, Writing—Reviewing and Editing; F.L. and Z.Y.: Conceptualization, Validation, Resources, Project Administration, Supervision, Funding Acquisition, Writing—Reviewing and Editing. All authors have read and agreed to the published version of the manuscript.

**Funding:** This research was funded by the Research Council of Norway under the industrial PhD scheme project number 311678 and Beyond AS.

**Acknowledgments:** The authors acknowledge the Research Council of Norway (NFR) and Beyond AS for funding this project under the industrial PhD scheme, project number 311678.

**Conflicts of Interest:** Obinna Egwu Eleri and Fengliu Lou are employed by Beyond AS, a Norwegian battery manufacturer. The remaining authors declare that the research was conducted in the

absence of any commercial or financial relationships that could be construed as a potential conflict of interest.

## References

1. Simon, P.; Gogotsi, Y. Materials for electrochemical capacitors. *Nat. Mater.* **2008**, *7*, 845. [[CrossRef](#)]
2. Simon, P.; Gogotsi, Y.; Dunn, B. Where do batteries end and supercapacitors begin? *Science* **2014**, *343*, 1210–1211. [[CrossRef](#)]
3. Amatucci, G.G.; Badway, F.; Du Pasquier, A.; Zheng, T. An asymmetric hybrid nonaqueous energy storage cell. *J. Electrochem. Soc.* **2001**, *148*, A930. [[CrossRef](#)]
4. Li, B.; Zheng, J.; Zhang, H.; Jin, L.; Yang, D.; Lv, H.; Shen, C.; Shellikeri, A.; Zheng, Y.; Gong, R. Electrode materials, electrolytes, and challenges in nonaqueous lithium-ion capacitors. *Adv. Mater.* **2018**, *30*, 1705670. [[CrossRef](#)]
5. Smith, P.H.; Tran, T.N.; Jiang, T.L.; Chung, J. Lithium-ion capacitors: Electrochemical performance and thermal behavior. *J. Power Sources* **2013**, *243*, 982–992. [[CrossRef](#)]
6. Ding, J.; Hu, W.; Paek, E.; Mitlin, D. Review of hybrid ion capacitors: From aqueous to lithium to sodium. *Chem. Rev.* **2018**, *118*, 6457–6498. [[CrossRef](#)] [[PubMed](#)]
7. Wang, H.; Zhu, C.; Chao, D.; Yan, Q.; Fan, H.J. Nonaqueous hybrid lithium-ion and sodium-ion capacitors. *Adv. Mater.* **2017**, *29*, 1702093. [[CrossRef](#)]
8. Shi, Z.; Zhang, J.; Wang, J.; Shi, J.; Wang, C. Effect of the capacity design of activated carbon cathode on the electrochemical performance of lithium-ion capacitors. *Electrochim. Acta* **2015**, *153*, 476–483. [[CrossRef](#)]
9. Sivakkumar, S.R.; Pandolfo, A. Evaluation of lithium-ion capacitors assembled with pre-lithiated graphite anode and activated carbon cathode. *Electrochim. Acta* **2012**, *65*, 280–287. [[CrossRef](#)]
10. Zhu, B.; Liu, B.; Qu, C.; Zhang, H.; Guo, W.; Liang, Z.; Chen, F.; Zou, R. Tailoring biomass-derived carbon for high-performance supercapacitors from controllably cultivated algae microspheres. *J. Mater. Chem. A* **2018**, *6*, 1523–1530. [[CrossRef](#)]
11. Magar, S.D.; Leibing, C.; Gómez-Urbano, J.L.; Cid, R.; Carriazo, D.; Balducci, A. Brewery waste derived activated carbon for high performance electrochemical capacitors and lithium-ion capacitors. *Electrochim. Acta* **2023**, *446*, 142104. [[CrossRef](#)]
12. Falco, C.; Sieben, J.M.; Brun, N.; Sevilla, M.; Van der Maelen, T.; Morallón, E.; Cazorla-Amorós, D.; Titirici, M.M. Hydrothermal carbons from hemicellulose-derived aqueous hydrolysis products as electrode materials for supercapacitors. *ChemSusChem* **2013**, *6*, 374–382. [[CrossRef](#)] [[PubMed](#)]
13. Kleszyk, P.; Ratajczak, P.; Skowron, P.; Jagiello, J.; Abbas, Q.; Frackowiak, E.; Béguin, F. Carbons with narrow pore size distribution prepared by simultaneous carbonization and self-activation of tobacco stems and their application to supercapacitors. *Carbon* **2015**, *81*, 148–157. [[CrossRef](#)]
14. Xue, B.; Jin, L.; Chen, Z.; Zhu, Y.; Wang, Z.; Liu, X.; Wang, X. The template effect of silica in rice husk for efficient synthesis of the activated carbon based electrode material. *J. Alloys Compd.* **2019**, *789*, 777–784. [[CrossRef](#)]
15. Tong, Y.; Yang, J.; Li, J.; Cong, Z.; Wei, L.; Liu, M.; Zhai, S.; Wang, K.; An, Q. Lignin-derived electrode materials for supercapacitor applications: Progress and perspectives. *J. Mater. Chem. A* **2023**, *11*, 1061–1082. [[CrossRef](#)]
16. Dubey, P.; Shrivastav, V.; Maheshwari, P.H.; Sundriyal, S. Recent advances in biomass derived activated carbon electrodes for hybrid electrochemical capacitor applications: Challenges and opportunities. *Carbon* **2020**, *170*, 1–29. [[CrossRef](#)]
17. Zou, K.; Cai, P.; Cao, X.; Zou, G.; Hou, H.; Ji, X. Carbon materials for high-performance lithium-ion capacitor. *Curr. Opin. Electrochem.* **2020**, *21*, 31–39. [[CrossRef](#)]
18. Han, P.; Xu, G.; Han, X.; Zhao, J.; Zhou, X.; Cui, G. Lithium ion capacitors in organic electrolyte system: Scientific problems, material development, and key technologies. *Adv. Energy Mater.* **2018**, *8*, 1801243. [[CrossRef](#)]
19. Dos Reis, G.S.; Larsson, S.H.; de Oliveira, H.P.; Thyrel, M.; Claudio Lima, E. Sustainable biomass activated carbons as electrodes for battery and supercapacitors—A mini-review. *Nanomaterials* **2020**, *10*, 1398. [[CrossRef](#)]
20. Carrott, P.; Carrott, M.R. Lignin—from natural adsorbent to activated carbon: A review. *Bioresour. Technol.* **2007**, *98*, 2301–2312.
21. González-García, P. Activated carbon from lignocellulosics precursors: A review of the synthesis methods, characterization techniques and applications. *Renew. Sustain. Energy Rev.* **2018**, *82*, 1393–1414. [[CrossRef](#)]
22. Yahya, M.A.; Al-Qodah, Z.; Ngah, C.Z. Agricultural bio-waste materials as potential sustainable precursors used for activated carbon production: A review. *Renew. Sustain. Energy Rev.* **2015**, *46*, 218–235. [[CrossRef](#)]
23. Danish, M.; Ahmad, T. A review on utilization of wood biomass as a sustainable precursor for activated carbon production and application. *Renew. Sustain. Energy Rev.* **2018**, *87*, 1–21. [[CrossRef](#)]
24. Abioye, A.M.; Ani, F.N. Recent development in the production of activated carbon electrodes from agricultural waste biomass for supercapacitors: A review. *Renew. Sustain. Energy Rev.* **2015**, *52*, 1282–1293. [[CrossRef](#)]
25. Rashidi, N.A.; Yusup, S. A review on recent technological advancement in the activated carbon production from oil palm wastes. *Chem. Eng. J.* **2017**, *314*, 277–290. [[CrossRef](#)]
26. Conway, B.E. *Electrochemical Supercapacitors: Scientific Fundamentals and Technological Applications*; Springer Science & Business Media: Berlin/Heidelberg, Germany, 2013.
27. Helmholtz, H.V. Ueber einige Gesetze der Vertheilung elektrischer Ströme in körperlichen Leitern, mit Anwendung auf die thierisch-elektrischen Versuche (Schluss.). *Ann. Phys.* **1853**, *165*, 353–377. [[CrossRef](#)]
28. Gao, Y.; Yue, Q.; Gao, B.; Li, A. Insight into activated carbon from different kinds of chemical activating agents: A review. *Sci Total Environ.* **2020**, *746*, 141094. [[CrossRef](#)]

29. Ukanwa, K.; Patchigolla, K.; Sakrabani, R.; Anthony, E.; Mandavgane, S. A Review of Chemicals to Produce Activated Carbon from Agricultural Waste Biomass. *Sustainability* **2019**, *11*, 6204. [[CrossRef](#)]
30. Barbieri, O.; Hahn, M.; Herzog, A.; Kötz, R. Capacitance limits of high surface area activated carbons for double layer capacitors. *Carbon* **2005**, *43*, 1303–1310. [[CrossRef](#)]
31. Khomenko, V.; Raymundo-Piñero, E.; Béguin, F. High-energy density graphite/AC capacitor in organic electrolyte. *J. Power Sources* **2008**, *177*, 643–651. [[CrossRef](#)]
32. Eleri, O.E.; Azuatalam, K.U.; Minde, M.W.; Trindade, A.M.; Muthuswamy, N.; Lou, F.; Yu, Z. Towards high-energy-density supercapacitors via less-defects activated carbon from sawdust. *Electrochim. Acta* **2020**, *362*, 137152. [[CrossRef](#)]
33. Salitra, G.; Soffer, A.; Eliad, L.; Cohen, Y.; Aurbach, D. Carbon electrodes for double-layer capacitors I. Relations between ion and pore dimensions. *J. Electrochem. Soc.* **2000**, *147*, 2486. [[CrossRef](#)]
34. Salanne, M.; Rotenberg, B.; Naoi, K.; Kaneko, K.; Taberna, P.-L.; Grey, C.P.; Dunn, B.; Simon, P. Efficient storage mechanisms for building better supercapacitors. *Nat. Energy* **2016**, *1*, 16070. [[CrossRef](#)]
35. Zheng, W.; Li, Z.; Han, G.; Zhao, Q.; Lu, G.; Hu, X.; Sun, J.; Wang, R.; Xu, C. Nitrogen-doped activated porous carbon for 4.5 V lithium-ion capacitor with high energy and power density. *J. Energy Storage* **2022**, *47*, 103675. [[CrossRef](#)]
36. Sun, J.; Li, G.; Wang, Z.; Guo, H.; Li, X.; Yan, G.; Wang, J. Balancing the anions adsorption and intercalation in carbon cathode enables high energy density dual-carbon lithium-ion capacitors. *Carbon* **2022**, *200*, 28–37. [[CrossRef](#)]
37. Cho, M.-Y.; Kim, M.-H.; Kim, H.-K.; Kim, K.-B.; Yoon, J.R.; Roh, K.C. Electrochemical performance of hybrid supercapacitor fabricated using multi-structured activated carbon. *Electrochem. Commun.* **2014**, *47*, 5–8. [[CrossRef](#)]
38. Jain, A.; Jayaraman, S.; Ulaganathan, M.; Balasubramanian, R.; Aravindan, V.; Srinivasan, M.P.; Madhavi, S. Highly mesoporous carbon from Teak wood sawdust as prospective electrode for the construction of high energy Li-ion capacitors. *Electrochim. Acta* **2017**, *228*, 131–138. [[CrossRef](#)]
39. Li, G.; Yang, Z.; Yin, Z.; Guo, H.; Wang, Z.; Yan, G.; Liu, Y.; Li, L.; Wang, J. Non-aqueous dual-carbon lithium-ion capacitors: A review. *J. Mater. Chem. A* **2019**, *7*, 15541–15563. [[CrossRef](#)]
40. Dubal, D.P.; Ayyad, O.; Ruiz, V.; Gomez-Romero, P. Hybrid energy storage: The merging of battery and supercapacitor chemistries. *Chem. Soc. Rev.* **2015**, *44*, 1777–1790. [[CrossRef](#)]
41. Li, S.; Chen, J.; Cui, M.; Cai, G.; Wang, J.; Cui, P.; Gong, X.; Lee, P.S. A High-Performance Lithium-Ion Capacitor Based on 2D Nanosheet Materials. *Small* **2017**, *13*, 1602893. [[CrossRef](#)]
42. Laszlo, K.; Tombacz, E.; Josepovits, K. Effect of activation on the surface chemistry of carbons from polymer precursors. *Carbon* **2001**, *39*, 1217–1228. [[CrossRef](#)]
43. Lota, G.; Grzyb, B.; Machnikowska, H.; Machnikowski, J.; Frackowiak, E. Effect of nitrogen in carbon electrode on the supercapacitor performance. *Chem. Phys. Lett.* **2005**, *404*, 53–58. [[CrossRef](#)]
44. Lyu, L.; Seong, K.-d.; Ko, D.; Choi, J.; Lee, C.; Hwang, T.; Cho, Y.; Jin, X.; Zhang, W.; Pang, H. Recent development of biomass-derived carbons and composites as electrode materials for supercapacitors. *Mater. Chem. Front.* **2019**, *3*, 2543–2570. [[CrossRef](#)]
45. Li, B.; Dai, F.; Xiao, Q.; Yang, L.; Shen, J.; Zhang, C.; Cai, M. Nitrogen-doped activated carbon for a high energy hybrid supercapacitor. *Energy Environ. Sci.* **2016**, *9*, 102–106. [[CrossRef](#)]
46. Yang, M.; Zhong, Y.; Ren, J.; Zhou, X.; Wei, J.; Zhou, Z. Fabrication of high-power Li-ion hybrid supercapacitors by enhancing the exterior surface charge storage. *Adv. Energy Mater.* **2015**, *5*, 1500550. [[CrossRef](#)]
47. Ci, L.; Song, L.; Jin, C.; Jariwala, D.; Wu, D.; Li, Y.; Srivastava, A.; Wang, Z.; Storr, K.; Balicas, L. Atomic layers of hybridized boron nitride and graphene domains. *Nat. Mater.* **2010**, *9*, 430–435. [[CrossRef](#)] [[PubMed](#)]
48. Zhao, X.; Zhang, Q.; Zhang, B.; Chen, C.-M.; Xu, J.; Wang, A.; Su, D.S.; Zhang, T. Decorated resol derived mesoporous carbon: Highly ordered microstructure, rich boron incorporation, and excellent electrochemical capacitance. *RSC Adv.* **2013**, *3*, 3578–3584. [[CrossRef](#)]
49. Lee, Y.-J.; Uchiyama, Y.; Radovic, L.R. Effects of boron doping in low-and high-surface-area carbon powders. *Carbon* **2004**, *42*, 2233–2244. [[CrossRef](#)]
50. Kalijadis, A.; Đorđević, J.; Trtić-Petrović, T.; Vukčević, M.; Popović, M.; Maksimović, V.; Rakočević, Z.; Laušević, Z. Preparation of boron-doped hydrothermal carbon from glucose for carbon paste electrode. *Carbon* **2015**, *95*, 42–50. [[CrossRef](#)]
51. Enterría, M.; Pereira, M.; Martins, J.; Figueiredo, J. Hydrothermal functionalization of ordered mesoporous carbons: The effect of boron on supercapacitor performance. *Carbon* **2015**, *95*, 72–83. [[CrossRef](#)]
52. Hishiyama, Y.; Irumano, H.; Kaburagi, Y.; Soneda, Y. Structure, Raman scattering, and transport properties of boron-doped graphite. *Phys. Rev. B* **2001**, *63*, 245406. [[CrossRef](#)]
53. Jiang, H.; Shi, D.; Sun, X.; Wang, S.; Li, Y.; Chang, B.; Zhang, B.; Shao, Y.; Wu, Y.; Hao, X. Boron carbonitride lithium-ion capacitors with an electrostatically expanded operating voltage window. *ACS Appl. Mater. Interfaces* **2020**, *12*, 47425–47434. [[CrossRef](#)] [[PubMed](#)]
54. Zhu, C.-L.; Wang, H.-L.; Fan, W.-J.; Zhai, S.-L.; Wang, X.-J.; Shi, J.; Huang, M.-H.; Liu, S.; Li, Z.; Chen, J.-W. Large-scale doping-engineering enables boron/nitrogen dual-doped porous carbon for high-performance zinc ion capacitors. *Rare Met.* **2022**, *41*, 2505–2516. [[CrossRef](#)]
55. Liu, C.; Koyyalamudi, B.B.; Li, L.; Emani, S.; Wang, C.; Shaw, L.L. Improved capacitive energy storage via surface functionalization of activated carbon as cathodes for lithium ion capacitors. *Carbon* **2016**, *109*, 163–172. [[CrossRef](#)]

56. Li, X.-R.; Jiang, Y.-H.; Wang, P.-Z.; Mo, Y.; Li, Z.-J.; Yu, R.-J.; Du, Y.-T.; Zhang, X.-R.; Chen, Y. Effect of the oxygen functional groups of activated carbon on its electrochemical performance for supercapacitors. *New Carbon Mater.* **2020**, *35*, 232–243. [[CrossRef](#)]
57. Zhang, S.S. Effect of surface oxygen functionalities on capacitance of activated carbon in non-aqueous electrolyte. *J. Solid State Electrochem.* **2017**, *21*, 2029–2036. [[CrossRef](#)]
58. Ding, Z.; Trouillet, V.; Dsoke, S. Are functional groups beneficial or harmful on the electrochemical performance of activated carbon electrodes? *J. Electrochem. Soc.* **2019**, *166*, A1004. [[CrossRef](#)]
59. Zhou, H.; Peng, Y.; Wu, H.B.; Sun, F.; Yu, H.; Liu, F.; Xu, Q.; Lu, Y. Fluorine-rich nanoporous carbon with enhanced surface affinity in organic electrolyte for high-performance supercapacitors. *Nano Energy* **2016**, *21*, 80–89. [[CrossRef](#)]
60. Gao, Y.; Yang, Z.; Wang, Y.; Wang, X. Boosting capacitive storage of cathode for lithium-ion capacitors: Combining pore structure with P-doping. *Electrochim. Acta* **2021**, *368*, 137646. [[CrossRef](#)]
61. Hu, X.; Fan, M.; Zhu, Y.; Zhu, Q.; Song, Q.; Dong, Z. Biomass-derived phosphorus-doped carbon materials as efficient metal-free catalysts for selective aerobic oxidation of alcohols. *Green Chem.* **2019**, *21*, 5274–5283. [[CrossRef](#)]
62. Jiang, Z.-L.; Sun, H.; Shi, W.-K.; Cheng, J.-Y.; Hu, J.-Y.; Guo, H.-L.; Gao, M.-Y.; Zhou, H.; Sun, S.-G. P-Doped Hive-like Carbon Derived from Pinecone Biomass as Efficient Catalyst for Li-O<sub>2</sub> Battery. *ACS Sustain. Chem. Eng.* **2019**, *7*, 14161–14169. [[CrossRef](#)]
63. Zhu, Y.; Huang, Y.; Chen, C.; Wang, M.; Liu, P. Phosphorus-doped porous biomass carbon with ultra-stable performance in sodium storage and lithium storage. *Electrochim. Acta* **2019**, *321*, 134698. [[CrossRef](#)]
64. Chen, C.; Huang, Y.; Meng, Z.; Lu, M.; Xu, Z.; Liu, P.; Li, T. Experimental design and theoretical evaluation of nitrogen and phosphorus dual-doped hierarchical porous carbon for high-performance sodium-ion storage. *J. Mater. Sci. Technol.* **2021**, *76*, 11–19. [[CrossRef](#)]
65. Thangavel, R.; Kannan, A.G.; Ponraj, R.; Thangavel, V.; Kim, D.-W.; Lee, Y.-S. Nitrogen-and sulfur-enriched porous carbon from waste watermelon seeds for high-energy, high-temperature green ultracapacitors. *J. Mater. Chem. A* **2018**, *6*, 17751–17762. [[CrossRef](#)]
66. Xu, G.; Han, J.; Ding, B.; Nie, P.; Pan, J.; Dou, H.; Li, H.; Zhang, X. Biomass-derived porous carbon materials with sulfur and nitrogen dual-doping for energy storage. *Green Chem.* **2015**, *17*, 1668–1674. [[CrossRef](#)]
67. Ren, Y.; Zhang, J.; Xu, Q.; Chen, Z.; Yang, D.; Wang, B.; Jiang, Z. Biomass-derived three-dimensional porous N-doped carbonaceous aerogel for efficient supercapacitor electrodes. *Rsc Adv.* **2014**, *4*, 23412–23419. [[CrossRef](#)]
68. Fang, B.; Binder, L. Enhanced surface hydrophobisation for improved performance of carbon aerogel electrochemical capacitor. *Electrochim. Acta* **2007**, *52*, 6916–6921. [[CrossRef](#)]
69. Fang, B.; Wei, Y.Z.; Maruyama, K.; Kumagai, M. High capacity supercapacitors based on modified activated carbon aerogel. *J. Appl. Electrochem.* **2005**, *35*, 229–233. [[CrossRef](#)]
70. Fang, B.; Binder, L. A modified activated carbon aerogel for high-energy storage in electric double layer capacitors. *J. Power Sources* **2006**, *163*, 616–622. [[CrossRef](#)]
71. Wei, Y.-Z.; Fang, B.; Iwasa, S.; Kumagai, M. A novel electrode material for electric double-layer capacitors. *J. Power Sources* **2005**, *141*, 386–391. [[CrossRef](#)]
72. Fang, B.; Wei, Y.-Z.; Kumagai, M. Modified carbon materials for high-rate EDLCs application. *J. Power Sources* **2006**, *155*, 487–491. [[CrossRef](#)]
73. Molina-Sabio, M.; Rodriguez-Reinoso, F. Role of chemical activation in the development of carbon porosity. *Colloids Surf. A Physicochem. Eng. Asp.* **2004**, *241*, 15–25. [[CrossRef](#)]
74. Lua, A.C.; Lau, F.Y.; Guo, J. Influence of pyrolysis conditions on pore development of oil-palm-shell activated carbons. *J. Anal. Appl. Pyrolysis* **2006**, *76*, 96–102. [[CrossRef](#)]
75. Bóta, A.; László, K.; Nagy, L.G.; Copitzky, T. Comparative study of active carbons from different precursors. *Langmuir* **1997**, *13*, 6502–6509. [[CrossRef](#)]
76. Guo, C.-Y.; Wang, C.-y. Effects of microstructure of precursors on characteristics of pitch based activated carbons. *Microporous Mesoporous Mater.* **2007**, *102*, 337–340. [[CrossRef](#)]
77. Zhou, S.-Y.; Li, X.-H.; Wang, Z.-X.; Guo, H.-J.; Peng, W.-J. Effect of activated carbon and electrolyte on properties of supercapacitor. *Trans. Nonferrous Met. Soc. China* **2007**, *17*, 1328–1333. [[CrossRef](#)]
78. Aworn, A.; Thiravetyan, P.; Nakbanpote, W. Preparation and characteristics of agricultural waste activated carbon by physical activation having micro-and mesopores. *J. Anal. Appl. Pyrolysis* **2008**, *82*, 279–285. [[CrossRef](#)]
79. Li, Z.; Zhang, L.; Amirkhiz, B.S.; Tan, X.; Xu, Z.; Wang, H.; Olsen, B.C.; Holt, C.M.; Mitlin, D. Carbonized chicken eggshell membranes with 3D architectures as high-performance electrode materials for supercapacitors. *Adv. Energy Mater.* **2012**, *2*, 431–437. [[CrossRef](#)]
80. Kim, Y.J.; Abe, Y.; Yanagiura, T.; Park, K.C.; Shimizu, M.; Iwazaki, T.; Nakagawa, S.; Endo, M.; Dresselhaus, M.S. Easy preparation of nitrogen-enriched carbon materials from peptides of silk fibroins and their use to produce a high volumetric energy density in supercapacitors. *Carbon* **2007**, *45*, 2116–2125. [[CrossRef](#)]
81. Yun, Y.S.; Cho, S.Y.; Shim, J.; Kim, B.H.; Chang, S.J.; Baek, S.J.; Huh, Y.S.; Tak, Y.; Park, Y.W.; Park, S. Microporous carbon nanoplates from regenerated silk proteins for supercapacitors. *Adv. Mater.* **2013**, *25*, 1993–1998. [[CrossRef](#)]
82. Zhu, F.; Cao, W.; Song, W.; Peng, J.; Yang, N.; Niu, J.; Wang, F. Biomass-derived carbon prepared through a quadruple-functional-salt approach for application in K-ion capacitors. *Chem. Eng. J.* **2022**, *449*, 137561. [[CrossRef](#)]

83. White, R.J.; Antonietti, M.; Titirici, M.-M. Naturally inspired nitrogen doped porous carbon. *J. Mater. Chem.* **2009**, *19*, 8645–8650. [[CrossRef](#)]
84. Tarimo, D.J.; Oyedotun, K.O.; Sylla, N.F.; Mirghni, A.A.; Ndiaye, N.M.; Manyala, N. Waste chicken bone-derived porous carbon materials as high performance electrode for supercapacitor applications. *J. Energy Storage* **2022**, *51*, 104378. [[CrossRef](#)]
85. Fidelis, M.; de Moura, C.; Kabbas Junior, T.; Pap, N.; Mattila, P.; Mäkinen, S.; Putnik, P.; Bursać Kovačević, D.; Tian, Y.; Yang, B. Fruit seeds as sources of bioactive compounds: Sustainable production of high value-added ingredients from by-products within circular economy. *Molecules* **2019**, *24*, 3854. [[CrossRef](#)]
86. Raymundo-Piñero, E.; Cadek, M.; Béguin, F. Tuning carbon materials for supercapacitors by direct pyrolysis of seaweeds. *Adv. Funct. Mater.* **2009**, *19*, 1032–1039. [[CrossRef](#)]
87. Endo, M.; Kim, Y.; Ishii, K.; Inoue, T.; Nomura, T.; Miyashita, N.; Dresselhaus, M. Heat-treatment retention time dependence of polyvinylidenechloride-based carbons on their application to electric double-layer capacitors. *J. Mater. Res.* **2003**, *18*, 693–701. [[CrossRef](#)]
88. Niu, J.; Shao, R.; Liu, M.; Liang, J.; Zhang, Z.; Dou, M.; Huang, Y.; Wang, F. Porous carbon electrodes with battery-capacitive storage features for high performance Li-ion capacitors. *Energy Storage Mater.* **2018**, *12*, 145–152. [[CrossRef](#)]
89. Qian, T.; Huang, Y.; Zhang, M.; Xia, Z.; Liu, H.; Guan, L.; Hu, H.; Wu, M. Non-corrosive and low-cost synthesis of hierarchically porous carbon frameworks for high-performance lithium-ion capacitors. *Carbon* **2021**, *173*, 646–654. [[CrossRef](#)]
90. Yang, S.; Zhang, L.; Sun, J.; Li, K.; Zhao, S.; Zhao, D.; Wang, J.; Yang, C.; Wang, X.; Cao, B. Corn-cob-derived hierarchical porous activated carbon for high-performance lithium-ion capacitors. *Energy Fuels* **2020**, *34*, 16885–16892. [[CrossRef](#)]
91. Sennu, P.; Aravindan, V.; Ganesan, M.; Lee, Y.G.; Lee, Y.S. Biomass-derived electrode for next generation lithium-ion capacitors. *ChemSusChem* **2016**, *9*, 849–854. [[CrossRef](#)]
92. Chen, X.; Mu, Y.; Cao, G.; Qiu, J.; Zhang, W.; Zhang, Q.; Ming, H. Structure-activity relationship of carbon additives in cathodes for advanced capacitor batteries. *Electrochim. Acta* **2022**, *413*, 140165. [[CrossRef](#)]
93. Shellikeri, A.; Yturriaga, S.; Zheng, J.; Cao, W.; Hagen, M.; Read, J.; Jow, T.; Zheng, J. Hybrid lithium-ion capacitor with LiFePO<sub>4</sub>/AC composite cathode—long term cycle life study, rate effect and charge sharing analysis. *J. Power Sources* **2018**, *392*, 285–295. [[CrossRef](#)]
94. Hagen, M.; Cao, W.; Shellikeri, A.; Adams, D.; Chen, X.; Brandt, W.; Yturriaga, S.; Wu, Q.; Read, J.; Jow, T. Improving the specific energy of Li-ion capacitor laminate cell using hybrid activated Carbon/LiNi<sub>0.5</sub>Co<sub>0.2</sub>Mn<sub>0.3</sub>O<sub>2</sub> as positive electrodes. *J. Power Sources* **2018**, *379*, 212–218. [[CrossRef](#)]
95. Granados-Moreno, M.; Moreno-Fernández, G.; Mysyk, R.; Carriazo, D. A high-energy hybrid lithium-ion capacitor enabled by a mixed capacitive-battery storage LiFePO<sub>4</sub>-AC cathode and a SnP<sub>2</sub>O<sub>7</sub>-rGO anode. *Sustain. Energy Fuels* **2023**, *7*, 965–976. [[CrossRef](#)]
96. Böckenfeld, N.; Placke, T.; Winter, M.; Passerini, S.; Balducci, A. The influence of activated carbon on the performance of lithium iron phosphate based electrodes. *Electrochim. Acta* **2012**, *76*, 130–136. [[CrossRef](#)]
97. Sun, X.; Zhang, X.; Zhang, H.; Xu, N.; Wang, K.; Ma, Y. High performance lithium-ion hybrid capacitors with pre-lithiated hard carbon anodes and bifunctional cathode electrodes. *J. Power Sources* **2014**, *270*, 318–325. [[CrossRef](#)]
98. Yu, J.; Wang, X.; Peng, J.; Jia, X.; Li, L.; Chuan, X. Porous activity of biomass-activated carbon enhanced by nitrogen-dopant towards high-performance lithium ion hybrid battery-supercapacitor. *J. Electrochem. Soc.* **2021**, *168*, 120537. [[CrossRef](#)]
99. Lee, S.H. Smart Multi-Layer Architecture Electrodes for High Energy Density Lithium-Ion Capacitors. *Batter. Supercaps* **2023**, *6*, e202200380. [[CrossRef](#)]
100. Frackowiak, E.; Béguin, F. Carbon materials for the electrochemical storage of energy in capacitors. *Carbon* **2001**, *39*, 937–950. [[CrossRef](#)]
101. Béguin, F.; Frackowiak, E. *Carbons for Electrochemical Energy Storage and Conversion Systems*; CRC Press: Boca Raton, FL, USA, 2009.
102. Raymundo-Piñero, E.; Cadek, M.; Wachtler, M.; Béguin, F. Carbon nanotubes as nanotexturing agents for high power supercapacitors based on seaweed carbons. *ChemSusChem* **2011**, *4*, 943–949. [[CrossRef](#)] [[PubMed](#)]
103. Jäckel, N.; Weingarh, D.; Zeiger, M.; Aslan, M.; Grobelsek, I.; Presser, V. Comparison of carbon onions and carbon blacks as conductive additives for carbon supercapacitors in organic electrolytes. *J. Power Sources* **2014**, *272*, 1122–1133. [[CrossRef](#)]
104. Suarez-Martinez, I.; Grobert, N.; Ewels, C. Nomenclature of sp<sup>2</sup> carbon nanoforms. *Carbon* **2011**, *50*, 741–747. [[CrossRef](#)]
105. Hantel, M.; Presser, V.; McDonough, J.; Feng, G.; Cummings, P.T.; Gogotsi, Y.; Kötz, R. In situ electrochemical dilatometry of onion-like carbon and carbon black. *J. Electrochem. Soc.* **2012**, *159*, A1897. [[CrossRef](#)]
106. Spahr, M.E.; Goers, D.; Leone, A.; Stallone, S.; Grivei, E. Development of carbon conductive additives for advanced lithium ion batteries. *J. Power Sources* **2011**, *196*, 3404–3413. [[CrossRef](#)]
107. McDonough, J.K.; Frolov, A.I.; Presser, V.; Niu, J.; Miller, C.H.; Ubieta, T.; Fedorov, M.V.; Gogotsi, Y. Influence of the structure of carbon onions on their electrochemical performance in supercapacitor electrodes. *Carbon* **2012**, *50*, 3298–3309. [[CrossRef](#)]
108. Chen, C.-C.; Patra, J.; Wang, F.-M.; Lin, J.-Y.; Dong, Q.-F.; Su, Y.-S.; Chang, J.-K. Binder-controlled pore size distribution of carbon electrodes to mitigate self-discharge of supercapacitors. *Carbon* **2023**, *204*, 555–565. [[CrossRef](#)]
109. Tran, H.Y.; Wohlfahrt-Mehrens, M.; Dsoke, S. Influence of the binder nature on the performance and cycle life of activated carbon electrodes in electrolytes containing Li-salt. *J. Power Sources* **2017**, *342*, 301–312. [[CrossRef](#)]
110. Galek, P.; Róžański, J.; Fic, K. Toward better porous carbon-based electrodes by investigation of the viscoelastic properties of carbon suspension. *Chem. Eng. J.* **2023**, *463*, 142476. [[CrossRef](#)]

111. Pettinger, K.-H.; Dong, W. When does the operation of a battery become environmentally positive? *J. Electrochem. Soc.* **2016**, *164*, A6274. [[CrossRef](#)]
112. Zhang, Y.S.; Courtier, N.E.; Zhang, Z.; Liu, K.; Bailey, J.J.; Boyce, A.M.; Richardson, G.; Shearing, P.R.; Kendrick, E.; Brett, D.J. A review of lithium-ion battery electrode drying: Mechanisms and metrology. *Adv. Energy Mater.* **2022**, *12*, 2102233. [[CrossRef](#)]
113. Jow, T.R.; Xu, K.; Borodin, O.; Ue, M. *Electrolytes for Lithium and Lithium-Ion Batteries*; Springer: Berlin/Heidelberg, Germany, 2014; Volume 58.
114. Zhong, C.; Deng, Y.; Hu, W.; Qiao, J.; Zhang, L.; Zhang, J. A review of electrolyte materials and compositions for electrochemical supercapacitors. *Chem. Soc. Rev.* **2015**, *44*, 7484–7539. [[CrossRef](#)]
115. Divya, M.L.; Lee, Y.-S.; Aravindan, V. Glyme solvated Na and Li-ion capacitors based on co-intercalation process using pencil graphite as battery type electrode. *J. Power Sources* **2022**, *543*, 231823. [[CrossRef](#)]
116. Decaux, C.; Ghimbeu, C.M.; Dahbi, M.; Anouti, M.; Lemordant, D.; Béguin, F.; Vix-Guterl, C.; Raymundo-Pinero, E. Influence of electrolyte ion–solvent interactions on the performances of supercapacitors porous carbon electrodes. *J. Power Sources* **2014**, *263*, 130–140. [[CrossRef](#)]
117. ho Lee, C.; Jung, C. Enhancement of Li+ ions mobility on activated carbon electrode for lithium ion capacitor. *Electrochim. Acta* **2017**, *232*, 596–600. [[CrossRef](#)]
118. ho Lee, C.; Xu, F.; Jung, C. Influence of the electrolyte distribution near the micropores of the activated carbon (AC) electrode on high rate performance of high voltage capacitors. *Electrochim. Acta* **2014**, *131*, 240–244. [[CrossRef](#)]
119. Peljo, P.; Girault, H.H. Electrochemical potential window of battery electrolytes: The HOMO–LUMO misconception. *Energy Environ. Sci.* **2018**, *11*, 2306–2309. [[CrossRef](#)]
120. Zhang, T.; Fuchs, B.; Secchiaroli, M.; Wohlfahrt-Mehrens, M.; Dsoke, S. Electrochemical behavior and stability of a commercial activated carbon in various organic electrolyte combinations containing Li-salts. *Electrochim. Acta* **2016**, *218*, 163–173. [[CrossRef](#)]
121. Borodin, O.; Behl, W.; Jow, T.R. Oxidative stability and initial decomposition reactions of carbonate, sulfone, and alkyl phosphate-based electrolytes. *J. Phys. Chem. C* **2013**, *117*, 8661–8682. [[CrossRef](#)]
122. Naoi, K. ‘Nanohybrid capacitor’: The next generation electrochemical capacitors. *Fuel Cells* **2010**, *10*, 825–833. [[CrossRef](#)]
123. Eleri, O.E.; Huld, F.; Pires, J.; Tucho, W.M.; Schweigart, P.; Svensson, A.M.; Lou, F.; Yu, Z. Revealing mechanisms of activated carbon capacity fade in lithium-ion capacitors. *Electrochim. Acta* **2023**, *453*, 142359. [[CrossRef](#)]
124. Guo, K.; Qi, S.; Wang, H.; Huang, J.; Wu, M.; Yang, Y.; Li, X.; Ren, Y.; Ma, J. High-Voltage Electrolyte Chemistry for Lithium Batteries. *Small Sci.* **2022**, *2*, 2100107. [[CrossRef](#)]
125. He, M.; Su, C.-C.; Peebles, C.; Zhang, Z. The impact of different substituents in fluorinated cyclic carbonates in the performance of high voltage lithium-ion battery electrolyte. *J. Electrochem. Soc.* **2021**, *168*, 010505. [[CrossRef](#)]
126. Kato, K.; Rodrigues, M.-T.F.; Babu, G.; Ajayan, P.M. Revealing anion chemistry above 3V in Li-ion capacitors. *Electrochim. Acta* **2019**, *324*, 134871. [[CrossRef](#)]
127. Stepień, D.; Zhao, Z.; Dsoke, S. Shift to post-li-ion capacitors: Electrochemical behavior of activated carbon electrodes in li-, na-and k-salt containing organic electrolytes. *J. Electrochem. Soc.* **2018**, *165*, A2807. [[CrossRef](#)]
128. Eleri, O.E.; Pires, J.; Huld, F.T.; Lu, S.; Schweigart, P.; Svensson, A.M.; Lou, F.; Yu, Z. Enhanced activated carbon lithium-ion capacitor electrochemical stability through electrolyte dielectric optimisation. *Sustain. Energy Fuels* **2023**, *7*, 1846–1854. [[CrossRef](#)]
129. Xu, K. “Charge-transfer” process at graphite/electrolyte interface and the solvation sheath structure of Li+ in nonaqueous electrolytes. *J. Electrochem. Soc.* **2007**, *154*, A162. [[CrossRef](#)]
130. Xu, K.; Lam, Y.; Zhang, S.S.; Jow, T.R.; Curtis, T.B. Solvation sheath of Li+ in nonaqueous electrolytes and its implication of graphite/electrolyte interface chemistry. *J. Phys. Chem. C* **2007**, *111*, 7411–7421. [[CrossRef](#)]
131. Xu, K.; von Wald Cresce, A. Li+-solvation/desolvation dictates interphasial processes on graphitic anode in Li ion cells. *J. Mater. Res.* **2012**, *27*, 2327–2341. [[CrossRef](#)]
132. Chikaoka, Y.; Ochi, R.; Fujii, K.; Ariga, T.; Sakurai, M.; Matsumoto, A.; Ueda, T.; Iwama, E.; Naoi, K. Controlling the Phase Separation of Dimethyl Carbonate Solvents Using a Dual-Cation System: Applications in High-Power Lithium Ion-Based Hybrid Capacitors. *J. Phys. Chem. C* **2022**, *126*, 14389–14398. [[CrossRef](#)]
133. Shan, X.Y.; Wang, Y.; Wang, D.W.; Li, F.; Cheng, H.M. Armoring graphene cathodes for high-rate and long-life lithium ion supercapacitors. *Adv. Energy Mater.* **2016**, *6*, 1502064. [[CrossRef](#)]
134. Han, D.; Weng, Z.; Li, P.; Tao, Y.; Cui, C.; Zhang, L.; Lin, W.; Gao, Y.; Kong, D.; Yang, Q.-H. Electrode thickness matching for achieving high-volumetric-performance lithium-ion capacitors. *Energy Storage Mater.* **2019**, *18*, 133–138. [[CrossRef](#)]
135. Qin, H.; Chao, H.; Zhang, M.; Huang, Y.; Liu, H.; Cheng, J.; Cao, L.; Xu, Q.; Guan, L.; Teng, X. Precious potential regulation of carbon cathode enabling high-performance lithium-ion capacitors. *Carbon* **2021**, *180*, 110–117. [[CrossRef](#)]
136. Dsoke, S.; Fuchs, B.; Gucciardi, E.; Wohlfahrt-Mehrens, M. The importance of the electrode mass ratio in a Li-ion capacitor based on activated carbon and Li<sub>4</sub>Ti<sub>5</sub>O<sub>12</sub>. *J. Power Sources* **2015**, *282*, 385–393. [[CrossRef](#)]
137. Jin, L.; Guo, X.; Shen, C.; Qin, N.; Zheng, J.; Wu, Q.; Zhang, C.; Zheng, J.P. A universal matching approach for high power-density and high cycling-stability lithium ion capacitor. *J. Power Sources* **2019**, *441*, 227211. [[CrossRef](#)]
138. Zhang, X.; Zhang, X.; Sun, X.; An, Y.; Song, S.; Li, C.; Wang, K.; Su, F.; Chen, C.-M.; Liu, F. Electrochemical impedance spectroscopy study of lithium-ion capacitors: Modeling and capacity fading mechanism. *J. Power Sources* **2021**, *488*, 229454. [[CrossRef](#)]
139. Weingarh, D.; Foelske-Schmitz, A.; Kötz, R. Cycle versus voltage hold—Which is the better stability test for electrochemical double layer capacitors? *J. Power Sources* **2013**, *225*, 84–88. [[CrossRef](#)]

140. Weingarh, D.; Noh, H.; Foelske-Schmitz, A.; Wokaun, A.; Kötz, R. A reliable determination method of stability limits for electrochemical double layer capacitors. *Electrochim. Acta* **2013**, *103*, 119–124. [[CrossRef](#)]
141. Sun, X.; Zhang, X.; Wang, K.; An, Y.; Zhang, X.; Li, C.; Ma, Y. Determination strategy of stable electrochemical operating voltage window for practical lithium-ion capacitors. *Electrochim. Acta* **2022**, *428*, 140972. [[CrossRef](#)]
142. Zhang, S.S. Dual-carbon lithium-ion capacitors: Principle, materials, and technologies. *Batter. Supercaps* **2020**, *3*, 1137–1146. [[CrossRef](#)]
143. Huang, Z.; Deng, Z.; Zhong, Y.; Xu, M.; Li, S.; Liu, X.; Zhou, Y.; Huang, K.; Shen, Y.; Huang, Y. Progress and challenges of prelithiation technology for lithium-ion battery. *Carbon Energy* **2022**, *4*, 1107–1132. [[CrossRef](#)]
144. Holtstiege, F.; Bärman, P.; Nölle, R.; Winter, M.; Placke, T. Pre-Lithiation Strategies for Rechargeable Energy Storage Technologies: Concepts, Promises and Challenges. *Batteries* **2018**, *4*, 4. [[CrossRef](#)]
145. Dose, W.M.; Johnson, C.S. Cathode pre-lithiation/sodiation for next-generation batteries. *Curr. Opin. Electrochem.* **2022**, *31*, 100827. [[CrossRef](#)]
146. Arnaiz, M.; Shanmukaraj, D.; Carriazo, D.; Bhattacharjya, D.; Villaverde, A.; Armand, M.; Ajuria, J. A transversal low-cost pre-metallation strategy enabling ultrafast and stable metal ion capacitor technologies. *Energy Environ. Sci.* **2020**, *13*, 2441–2449. [[CrossRef](#)]
147. Park, M.-S.; Lim, Y.-G.; Kim, J.-H.; Kim, Y.-J.; Cho, J.; Kim, J.-S. A novel lithium-doping approach for an advanced lithium ion capacitor. *Adv. Energy Mater.* **2011**, *1*, 1002–1006. [[CrossRef](#)]
148. Park, M.S.; Lim, Y.G.; Hwang, S.M.; Kim, J.H.; Kim, J.S.; Dou, S.X.; Cho, J.; Kim, Y.J. Scalable integration of Li<sub>5</sub>FeO<sub>4</sub> towards robust, high-performance lithium-ion hybrid capacitors. *ChemSusChem* **2014**, *7*, 3138–3144. [[CrossRef](#)]
149. Jeżowski, P.; Crosnier, O.; Deunf, E.; Poizot, P.; Béguin, F.; Brousse, T. Safe and recyclable lithium-ion capacitors using sacrificial organic lithium salt. *Nat. Mater.* **2018**, *17*, 167–173. [[CrossRef](#)]
150. Sun, C.; Zhang, X.; Li, C.; Wang, K.; Sun, X.; Ma, Y. High-efficiency sacrificial prelithiation of lithium-ion capacitors with superior energy-storage performance. *Energy Storage Mater.* **2020**, *24*, 160–166. [[CrossRef](#)]
151. Pan, X.; Chojnacka, A.; Jeżowski, P.; Béguin, F. Na<sub>2</sub>S sacrificial cathodic material for high performance sodium-ion capacitors. *Electrochim. Acta* **2019**, *318*, 471–478. [[CrossRef](#)]
152. Pan, X.; Chojnacka, A.; Béguin, F. Gas free oxidation of NaCN for presodiating and stabilizing the anodic host of sodium-ion capacitors. *J. Energy Chem.* **2022**, *72*, 33–40. [[CrossRef](#)]
153. Jeżowski, P.; Chojnacka, A.; Pan, X.; Béguin, F. Sodium amide as a “zero dead mass” sacrificial material for the pre-sodiation of the negative electrode in sodium-ion capacitors. *Electrochim. Acta* **2021**, *375*, 137980. [[CrossRef](#)]
154. Pan, X.; Chojnacka, A.; Béguin, F. Advantageous carbon deposition during the irreversible electrochemical oxidation of Na<sub>2</sub>C<sub>4</sub>O<sub>4</sub> used as a presodiation source for the anode of sodium-ion systems. *Energy Storage Mater.* **2021**, *40*, 22–30. [[CrossRef](#)]
155. Shanmukaraj, D.; Grugeon, S.; Laruelle, S.; Douglade, G.; Tarascon, J.-M.; Armand, M. Sacrificial salts: Compensating the initial charge irreversibility in lithium batteries. *Electrochem. Commun.* **2010**, *12*, 1344–1347. [[CrossRef](#)]
156. Zhang, S.S. Eliminating pre-lithiation step for making high energy density hybrid Li-ion capacitor. *J. Power Sources* **2017**, *343*, 322–328. [[CrossRef](#)]

**Disclaimer/Publisher’s Note:** The statements, opinions and data contained in all publications are solely those of the individual author(s) and contributor(s) and not of MDPI and/or the editor(s). MDPI and/or the editor(s) disclaim responsibility for any injury to people or property resulting from any ideas, methods, instructions or products referred to in the content.